Monthly Notices of the ROYAL ASTRONOMICAL SOCIETY

MNRAS **522,** 4404–4420 (2023) https://doi.org/10.1093/mnras/stad1154
Advance Access publication 2023 April 25

Peeking beneath the precision floor – II. Probing the chemo-dynamical histories of the potential globular cluster siblings, NGC 288 and NGC 362

Stephanie Monty [1,2,3★] David Yong,[2,3] Davide Massari,[4] Madeleine McKenzie [2,3] GyuChul Myeong,[5] Sven Buder [2,3] Amanda I. Karakas [3,6] Ken C. Freeman,[2,3] Anna F. Marino [7,8] Vasily Belokurov [1] and N. Wyn Evans[1]

[1]*Institute of Astronomy, University of Cambridge, Madingley Rd, Cambridge CB3 0HA, UK*
[2]*Research School of Astronomy and Astrophysics, Mt Stromlo Observatory, Weston Creek, Australian Capital Territory 2611, Australia*
[3]*ARC Centre of Excellence for All Sky Astrophysics in 3 Dimensions (ASTRO 3D), Australia*
[4]*INAF - Osservatorio di Astrofisica e Scienza dello Spazio di Bologna, Via Gobetti 93/3, I-40129 Bologna, Italy*
[5]*Harvard-Smithsonian Center for Astrophysics, 60 Garden Street, Cambridge, MA 02138, USA*
[6]*School of Physics & Astronomy, Monash University, Clayton, Victoria 3800, Australia*
[7]*Instituto Nazionale di Astrofisica - Osservatorio Astronomico di Padova, Vicolo dell'Osservatorio 5, I-35122 Padua, Italy*
[8]*Instituto Nazionale di Astrofisica - Osservatorio Astrofisico di Arcetri, Largo Enrico Fermi, 5, I-50125 Firenze, Italy*

Accepted 2023 February 4. Received 2023 January 25; in original form 2022 November 20

ABSTRACT

The assembly history of the Milky Way (MW) is a rapidly evolving subject, with numerous small accretion events and at least one major merger proposed in the MW's history. Accreted alongside these dwarf galaxies are globular clusters (GCs), which act as spatially coherent remnants of these past events. Using high precision differential abundance measurements from our recently published study, we investigate the likelihood that the MW clusters NGC 362 and NGC 288 are galactic siblings, accreted as part of the *Gaia*-Sausage-Enceladus (GSE) merger. To do this, we compare the two GCs at the 0.01 dex level for 20 + elements for the first time. Strong similarities are found, with the two showing chemical similarity on the same order as those seen between the three LMC GCs, NGC 1786, NGC 2210-, and NGC 2257. However, when comparing GC abundances directly to GSE stars, marked differences are observed. NGC 362 shows good agreement with GSE stars in the ratio of Eu to Mg and Si, as well as a clear dominance in the *r*- compared to the *s*-process, while NGC 288 exhibits only a slight *r*-process dominance. When fitting the two GC abundances with a GSE-like galactic chemical evolution model, NGC 362 shows agreement with both the model predictions and GSE abundance ratios (considering Si, Ni, Ba, and Eu) at the same metallicity. This is not the case for NGC 288. We propose that the two are either not galactic siblings, or GSE was chemically inhomogeneous enough to birth two similar, but not identical clusters with distinct chemistry relative to constituent stars.

Key words: techniques: spectroscopic – stars: abundances – globular clusters: general – globular clusters: individual: NGC 288 – globular clusters: individual: NGC 362 – Galaxy: formation.

1 INTRODUCTION

Recent data release from the *Gaia* mission (DR2, EDR3, DR3, Gaia Collaboration et al. 2018, 2021, 2022) have triggered a revolution in our understanding of the assembly history of the Milky Way (MW). Leveraging this unprecedented data set of nearby stars, a plethora of past merger events between the MW and dwarf galaxies (dGals) have been proposed (e.g. Belokurov et al. 2018; Haywood et al. 2018; Helmi et al. 2018; Koppelman et al. 2019; Kruijssen et al. 2019; Massari, Koppelman & Helmi 2019; Myeong et al. 2019; Forbes 2020; Naidu et al. 2020; Horta et al. 2021). Along with the dGals themselves, each of these merger events is likely to have brought in a system of associated globular clusters (GCs) (Searle & Zinn 1978; Mackey & Gilmore 2004; Abadi, Navarro & Steinmetz 2006; Law & Majewski 2010; Trujillo-Gomez et al. 2021; Rostami Shirazi et al. 2022). And while these accreted dGals have long since been disrupted, distributing their constituent stars across the MW, some members of their GC systems have likely remained intact. Identifying and characterising the GC systems of these long-gone dGals could provide a chemo-dynamical link to these past merger events.

Prior to *Gaia*, classifying the MW's population of GCs as a means of inferring their origins was largely reliant on the GC age-metallicity relation (AMR, Marín-Franch et al. 2009; Forbes & Bridges 2010). Coupling the AMR with GC kinematics subsequently strengthened the proposed distinction between accreted versus *in situ* GCs (Leaman, VandenBerg & Mendel 2013). Old, metal-poor clusters were found to generally exhibit halo kinematics and were proposed to have been accreted, while younger, more metal-rich clusters showed disc kinematics and were proposed to have formed *in situ* with the MW. The separation of these populations was further supported via their different [Si,Ca/Fe] abundances as shown by Recio-Blanco (2018), with old, metal-poor clusters occupying a plateau in [Si,Ca/Fe].

★ E-mail: sm2744@cam.ac.uk

Thanks to the incredibly high quality of the *Gaia* DR2/DR3 data (Gaia Collaboration et al. 2018, 2022), revised GC parallaxes and proper motions are now available to calculate precise cluster orbits. Using revised GC orbital characteristics (e.g. orbital energy, the z-component of angular momentum and/or orbital actions), studies by Myeong et al. (2018), Myeong et al. (2019), and Massari et al. (2019) classified GCs as having been accreted alongside proposed accretion events, including the Sequoia and *Gaia*−Sausage−Enceladus (Gaia-Sausage/GSE, Belokurov et al. 2018; Helmi et al. 2018).[1], or as having formed *in situ* alongside the progenitor of the MW disc. This has since expanded with the discovery of additional accretion events and the release of EDR3 (Callingham et al. 2022; Limberg et al. 2022; Malhan et al. 2022).

Thus far, dynamical associations of GCs to merger events has involved integrating GC orbits within a static potential (without a live halo composed of particles). The associations are then made when clusters are found to group together in the dynamical spaces associated with proposed progenitors. However, groups in dynamical spaces sometimes overlap, making the associations uncertain. Moreover, further complexity can be introduced when considering live halos, particularly in energy versus z-angular momentum space (Pagnini et al. 2022). Unfortunately, until now their chemical abundances have not yielded greater clarity, revealing no distinct differences between clusters from proposed events (Horta et al. 2020).

Using catalogues of GC stars within the APOGEE survey (Majewski et al. 2017), Horta et al. (2020) tagged GCs to different accretion events in energy versus z-angular momentum space following the convention of Massari et al. (2019). When examining the average cluster abundances in the α-elements Si and Mg (elements largely associated with nucleosynthesis via core-collapse supernovae), they found no distinctions between GCs tagged to different events. This is despite a clear difference in α-element abundances being seen between *in situ* and accreted MW GCs (Recio-Blanco 2018) and is likely the result of limited chemical abundance precision. Given that studies have shown that GSE field stars occupy both a unique region of chemical as well as dynamical space with respect to MW field stars (Haywood et al. 2018; Matsuno, Aoki & Soda 2019; Feuillet et al. 2020; Monty et al. 2020; Aguado et al. 2021; Feuillet et al. 2021; Matsuno et al. 2021; Buder et al. 2022; Horta et al. 2022), and evidence of the chemical distinction among proposed accreted substructure is emerging (Horta et al. 2022; Matsuno et al. 2022a, b), chemical homogeneity of different GC populations seems unlikely.

In addition to the wealth of quality information large spectroscopic surveys can provide, we owe a major discovery in the MW to a small study that pushed the chemical precision floor to a new limit. The discovery by Nissen & Schuster (2010) that the MW hosts two distinct halo populations, a high- and low-α sequence (and the assertion that these represent the *in situ* and accreted halo populations) was only possible due to measurement errors on the order 0.01 dex. This was achieved through performing differential abundance measurements, a technique pioneered in the study of solar twins (Meléndez et al. 2009). Another example is the discovery that the seemingly disc-like GC NGC 6752 hosts star-to-star abundance variations at the two sigma level for every element measured, in addition to significant correlations between unexpected elements (Yong et al. 2013). This can only be explained by invoking a specific enrichment pattern in the (pre)proto-cluster environment, providing a direct link to the cluster's parent galaxy.

Continuing with the exploration of MW GCs in the high precision regime, we conducted a differential chemical abundance study of the two clusters NGC 288 and NGC 362. The two clusters are particularly interesting as they have nearly identical metallicities (NGC 288: [Fe/H] ~ -1.39, NGC 362: [Fe/H] ~ -1.33, Shetrone & Keane 2000) and orbital characteristics (e.g. NGC 288: $(r_{\rm peri}, r_{\rm apo}) = (3.33, 13.01)$ kpc, NGC 362: $(r_{\rm peri}, r_{\rm apo}) = (1.05, 12.48)$ kpc and both are on weakly retrograde orbits, Baumgardt et al. 2019a) and yet they are chemically distinct (Shetrone & Keane 2000; Carretta et al. 2013) and show clear signs of different dynamical evolution (Dalessandro et al. 2013; Piatti 2018; Sollima 2020). Using integrals of motion space (Helmi & de Zeeuw 2000), Massari et al. (2019) classified both clusters as having been accreted in the GSE merger, while Myeong et al. (2018, 2019) lists NGC 362 as having a possible association with the *Gaia*-Sausage event and NGC 288 as having no association.

This is the second paper in a series using differential analysis to probe the chemistry of NGC 288 and NGC 362. In our first paper (Monty et al. 2023, hereafter Paper I), we explored the chemistry in the two clusters in the context of GC chemical evolution. Our analysis revealed statistically significant dispersion in several elements in both clusters including, Fe I and heavy elements from the slow neutron capture (s-process) nucleosynthetic group.

In addition to a spread in the s-process elements, NGC 362 displayed a spread in the heavy element Eu, a member of the rapid neutron capture (r-process) nucleosynthetic group (Burbidge et al. 1957). Furthermore, using a spread in s-process elements, we identified two distinct groups within NGC 362 which we believe are associated with separate star formation (SF) events. The older, s-process weak population was found to be dominated by the r-process with a differential $\Delta^{\rm La} - \Delta^{\rm Eu}$[2] ratio of -0.16 ± 0.06. We then proposed that the r-process enrichment and dispersion found within the older group were primordial. This discovery motivated further research into whether primordial GC abundances reflect the abundances of their host galaxies. Can the two be linked?

In this study, we explore the possibility that the two GCs, NGC 288 and NGC 362, are galactic siblings accreted as part of the same event. To investigate this question, we make use of high precision differential abundance measurements from our previous study of NGC 288 and NGC 362 (Paper I, discussed in Section 2) to compare and contrast the two. Section 3 explores both scenarios using chemo-dynamical evidence that suggests that the GCs are (Section 3.1.1 and 3.1.2) and are not siblings (Sec.s 3.2.1 and 3.2.2). Without assuming an accretion scenario, in Section 4 we assess the fit of a GSE-tailored galactic chemical evolution model to six different abundance ratios in our GCs. Finally, in Section 5 we summarize the results of our investigation and provide conclusions as to the potential origin of the two GCs in Section 6.

2 SUMMARY OF OBSERVATIONS AND ANALYSIS FROM PAPER I

In Paper I we used the technique of differential abundance analysis to measure Na, Al, Mg, Si, Ca, Ti, Cr, Fe, Co, Ni, Cu, Zn, Sr, Y, Zr, Ba, La, Ce, Nd, and Eu in NGC 288 and NGC 362. Six red giant

[1]Note that while the *Gaia* Sausage and Enceladus events share many member stars in common and occupy similar, but not identical regions of E versus L_z space, they have distinctly different progenitor scenarios and in-fall orbits. We will endeavour to discuss the two separately where possible.

[2]Note that we use the $\Delta^{\rm X}$ notation when referring to differential or relative abundance ratios. This is analogous to the traditional [X/Fe] notation used in spectroscopic studies. Further explanation is given in Section 2

branch (RGB) stars from the tip of the RGB in NGC 288 and eight from NGC 362 from the study of Shetrone & Keane (2000) were selected to re-observe using the VLT/UVES ($R \sim 110\,000$, Dekker et al. 2000). The star mg9 (also known as B3169: Buonanno et al. 1986) was selected from the pioneering study of Yong et al. (2013) to use as a reference star for the analysis.

Briefly, differential abundance analysis exploits the selection of 'stellar siblings', stars with similar stellar parameters (effective temperature, $T_{\rm eff}$, surface gravity, log g and metallicity expressed as [Fe/H]) to minimize systematic errors amongst the program and reference stars (see Nissen & Gustafsson 2018, for a review of the technique). The software `q2` (Ramírez et al. 2014) was used to perform the analysis, in tandem with the radiative transfer code `MOOG` (Sneden 1973) using `MARCS` (Gustafsson et al. 2008) model atmospheres. Ultimately, relative abundance errors on the order 0.01–0.02 dex were recovered in both clusters with the smallest uncertainties being associated with Fe I in both clusters (0.01 dex in NGC 288 and 0.016 dex in NGC 362.) Further details of the abundance analysis, determination of stellar parameters and line list can be found throughout Section 2 in Paper I.

3 CHEMODYNAMICS: IN THE CONTEXT OF MILKY WAY EVOLUTION

In this section we use chemo-dynamical evidence to explore two possibilities regarding the origin of the clusters. The first, is that the two GCs formed in the same dGal and were accreted as part of the *same* merger event, in essence that they are 'galactic siblings'. And the second, is that they did not originate from the same dGal and instead joined the MW via different accretion scenarios.

3.1 Accretion scenario I: galactic siblings

We begin our exploration of the cluster accretion histories by discussing the possibility that they formed alongside the same host dGal and therefore joined the MW as part of the same accretion event. As discussed in Section 1, this scenario has been proposed for these two clusters by Massari et al. (2019), with the two clusters brought in as part of the GSE merger. Callingham et al. (2022) and Limberg et al. (2022) further support this classification, assigning both NGC 288 and NGC 362 as GSE GCs with 100 per cent certainty in their models. Malhan et al. (2022) also support the sibling scenario, but assign NGC 288 and NGC 362 to a separate accretion event termed 'Pontus'. Pontus is proposed to have been accreted ∼1 Gyr before GSE (Malhan 2022; Hammer et al. 2023). To support this theory, we experiment with classifying the clusters dynamically within a four component MW potential and compare the scale of chemical similarities between the two clusters to those found between known galactic siblings within the Large Magellanic Cloud (LMC) GC system.

3.1.1 Dynamical support for the sibling scenario

The studies of Massari et al. (2019) and Callingham et al. (2022) assign cluster association primarily based on the two GCs occupying a similar region of energy (E) versus the z-component of angular momentum (L_z) space. In the case of Callingham et al. (2022) and Limberg et al. (2022), actions **J** were also used. The location of the two GCs in solar-scaled E versus L_z space is shown in Fig. 1 after integration in the `McMillan17` potential of McMillan (2017) and the MW potential `MWPotential2014` of Bovy (2015) for 2 Gyr.

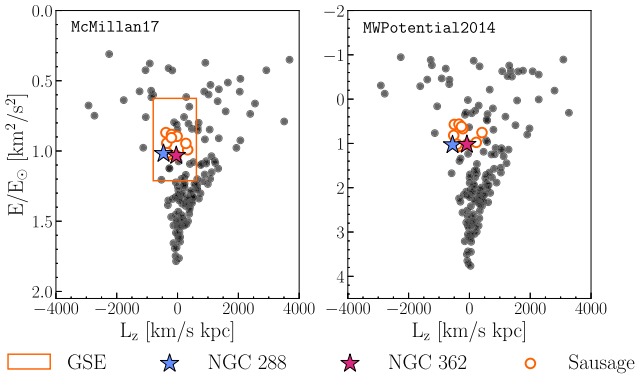

Figure 1. Energy (E in km^2/s^2) scaled by solar energy versus angular momentum (L$_z$ in km/s2 kpc) for the majority of MW GCs calculated using the `McMillan17` MW potential (as in the studies of Myeong et al. 2018; Massari et al. 2019), integrating for 2 Gyr (*left*). The extent of GSE in E versus L$_z$ as defined by Massari et al. (2019) is marked in orange, while the Sausage GCs identified by Myeong et al. (2018) are shown as the open orange circles. NGC 288 and NGC 362 are shown as the blue and pink stars, respectively. The same information is shown for GCs integrated in the `MWPotential2014` MW potential (right).

The solar energy values used to scale the y-axes in Fig. 1 were calculated in the respective potentials, illustrating a fundamental difference between the two −-the component masses. A collection of MW GCs is also plotted in the background of Fig. 1. An orange box is placed around GSE using the limits from Massari et al. (2019) (calculated in the `McMillan17` potential), while orange open circles mark all the proposed Sausage GCs from Myeong et al. (2018) −-note that there is not complete overlap between the two proposed events (see the footnote in Section 1). The similar location of the two GCs in E versus L_z implies that the two must share many orbital characteristics in common, which is indeed the case.

Using the *Gaia* EDR3 proper motions and parallax distances for the GCs as determined by Vasiliev & Baumgardt (2021) we have re-determined the orbital parameters of the two GCs. To do this we use the `MWPotential2014` potential in `galpy` (Bovy 2015) and orient ourselves in the usual way. That is, we assume the sun is 20.8 pc above the galactic plane (Bennett & Bovy 2019), the distance to the solar circle is 8.178 kpc (GRAVITY Collaboration et al. 2019) and that circular velocity at the solar circle is 229 km/s (Eilers et al. 2019). We integrate the orbits forwards and backwards for 5 Gyr and recover similar pericentric and apocentric radii for the two GCs ($r_{\rm peri} = 0.25$ kpc and $r_{\rm apo} = 10.90$ kpc for NGC 288 and $r_{\rm peri} = 0.38$ kpc and $r_{\rm apo} = 13.17$ kpc for NGC 362.) Additionally, the two GCs are found to have similar orbital eccentricities (NGC 288: $e = 0.64$ and NGC 362: $e = 0.84$) and orbital periods. Finally, in the axisymmetric, time-invariant `MWPotential2014` potential, the GCs share similar values of E, L_z and actions as one would expect.

Both Massari et al. (2019) and Callingham et al. (2022) derive their 'tagging' characteristics, E and L_z (and **J**) under the assumption of a time-invariant, axisymmetric potential (the conditions under which all of these quantities are conserved). Both studies assume the MW potential of McMillan (2017) as implemented in `AGAMA` (Vasiliev 2019)[3] In reality, the MW potential is neither time invariant, nor symmetric in the inner regions due to the presence of the MW bar.

[3]The McMillan (2017) potential does not include a component for the bar and instead only models the bulge, disc, and dark matter (DM) halo. See Tables 1 and 4 in McMillan (2017) for characteristics of each component.

Table 1. Characteristics of the two Dehnen bars (DBP) and our Ferrers (FP) potential bulge-bar used to explore perturbations to the orbits of our two GCs in Section 3.1.1. The two Dehnen bars are defined by the bar pattern speed (Ω_b), bar radius (R_b), and bar strength (A_f). Characteristics for the strong Dehnen bar are taken from the simulation parameters of Monari et al. (2016) and characteristics for the weak bar from the range of derived values in Wegg, Gerhard & Portail (2015). Our Ferrers (FP) potential ellipsoid is defined by the total bar + bulge mass $M_{bar+bulge}$, scale radius (a) and major- and minor-axis ratio (e), with the major axis sitting in the Y-X plane.

Potential	Ω_b km/s/kpc	R_b kpc	A_f km^2/s^2	$M_{bar+bulge}$ 10^{10} $M_\odot$	a kpc	e
DBP (strong)	52	3.4	2101	...	...	...
DBP (weak)	40	5.1	621	...	...	...
FP	40	5.1	...	2	5	0.2

Many of the orbits of the MW GCs, including NGC 288 and NGC 362 pass within the inner region of the MW where they are subject to the effects of the bar (recent estimates of the bar co-rotation radius are $6.5 < R_{CR} < 7.5$ kpc, Clarke & Gerhard 2022). This raises the issue of whether the presence of a bar would impact the tagging of the two clusters by changing the orbital characteristics. While testing the impact of a time-variable potential is non-trivial, we can explore the impact of adding a model bar to our MW potential.

We explored two different models for the bar, using the `galpy` implementation of Dehnen's Bar in 3D (`DehnenBarPotential`, Dehnen 2000; Monari et al. 2016) and the `galpy` implementation of Ferrers potential (`FerrersPotential`, Ferrers 1877). In the case of the Dehnen potential this is added to the three component potential of `MWPotential2014` (representing the MW bulge, disc, and dark matter halo). We adopt `MWPotential2014` for this exercise as the form of the potential components make the addition of a static bar fairly simple. In the case of Ferrers potential, which models both the bulge and the bar as an ellipsoid, the potential is built from the halo and disc components of `MWPotential2014` with the addition of `FerrersPotential`.

To build our Dehnen bars we select characteristics for both a strong and weak bar and investigate the impact of both on the cluster parameters. For Ferrers potential, we only experiment with a weak bar. Characteristics of the three bar models are listed in Table 1. Three example orbits for NGC 288 over the 10 Gyr total integration time are shown in Fig. 2, in the Y-X, Z-X, and Z-R planes for different choices of the potential. NGC 288 was chosen to demonstrate the orbital differences as the changes to the orbit were more severe overall when compared to NGC 362 (for completeness the orbital changes to NGC 362 are shown in Fig. B1). The top-most plot shows the orbit integrated in the `MWPotential2014` potential, the middle, and bottom-most plots show the orbit integrated in the `MWPotential2014 + DehnenBarPotential` potential with weak and strong bar characteristics respectively.

Despite the orbits showing some differences in Fig. 2, across the three different implementations of the Dehnen bar potential, no significant change in the 'tagging' parameters E and L_z was observed. To explore whether the tagging of the two GCs has changed under the addition of the bar, we focus on the change in L_z across potentials. This is because energy is highly sensitive to the mass differences between the `MWPotential2014` and the `McMillan17` potential.

Subject to the `MWPotential2014` potential, the angular momentum of the two GCs is $L_z = -41.39$ km/s kpc (NGC 288) and $L_z = -89.14$ km/s kpc (NGC 362), well within the range associated with the GSE merger as identified by Massari et al. (2019) ($-800 < L_z < 620$ km/s kpc). Subject to our bar modeled using Ferrers potential, this changes to $L_z = -187.83$ km/s kpc for NGC 288 and $L_z = -93.31$ km/s kpc for NGC 362. Finally, under our weak and strong Dehnen Bar respectively, the L_z ranges from -31.49 km/s kpc to -70.48 km/s kpc for NGC 288 and -70.79 km/s kpc to -93.06 km/s kpc for NGC 362. Again, these values are well within the range of L_z associated with GSE as given by Massari et al. (2019) and Helmi et al. (2018). Conceptually one can see the impact of the bar 'spinning up' the GCs as they interact with the bar, with the stronger bar causing more spin up. As an experiment, we integrated both clusters forwards for an additional 5 Gyr and saw an additional increase of 30–50 km/s kpc in L_z in both clusters.

Our first conclusion is that in the presence of a bar as we have modeled it and without exploring a time variable potential, the GCs retain their dynamical association to GSE, supporting the idea that they could be galactic siblings.

3.1.2 *Chemical support for the sibling scenario*

To investigate the chemical similarities between the two clusters we split NGC 362 into the two *s*-process groups (*s*-rich and *s*-weak) discovered in Paper I and compare both groups to NGC 288. As discussed in Section 1, two distinct groups were found within NGC 362 separated by ∼0.3 dex in their mean *s*-process abundances ($\Delta^{Y,\,Ba,\,La}$). Each group contains four stars, with the *s*-rich group also containing the extremely *s*-process enhanced star NGC362-1441 (∼0.2 dex more enriched than the remainder of the *s*-rich group) discovered in Paper I. A review of nucleosynthetic sites of the *s*-process is given in Section 3.1.4 in Paper I (the classification of nucleosynthetic groups follows the system set out by the seminal paper of Burbidge et al. 1957). Briefly, the main site of the *s*-process, contributing predominately to the production of elements from Sr to Nd, is asymptotic giant branch stars (AGBs, Busso, Gallino & Wasserburg 1999; Karakas 2010; Karakas & Lattanzio 2014; Kobayashi, Karakas & Lugaro 2020).

In Paper I, the average chemical abundances measured in NGC 288 showed good agreement with the average abundances measured in the *s*-weak group. We also used two lines of evidence to infer that the *s*-rich group may be younger than the *s*-weak group (see Section 4 of Paper I). If we accept the *s*-weak group as the older and primordial group in NGC 362, comparisons between the *s*-weak group and NGC 288 hinted at primordial similarities between the two clusters. We explore this idea further in the top panel of Fig. 3, where an element-by-element comparison between both *s*-process group and NGC 288 is presented. In the panel, the open circles show the abundance difference between NGC 288 and the *s*-rich group in NGC 362, while the filled circles represent abundance differences between NGC 288 and the *s*-weak group in NGC 362.

To evaluate the differences we take a simple approach by calculating the average (differential) abundance for each well-measured element (n lines > 2, with the exception of Eu and neglecting the light elements) in each cluster and then calculate the absolute difference. The error on the cluster-to-cluster difference is defined as the sum in quadrature of the average error in that element, in each cluster. The first thing to notice is the confirmation of the conclusion from Paper I that the *s*-weak group and NGC 288 show greater similarity than the *s*-rich group and NGC 288 (13 of the 20 elements show greater similarity as shown in Fig. 3).

The heavy *s*-process abundances (Ba and heavier) within the two 'primordial' populations is strikingly similar, as well as the light elements (particularly Si through to Ti). The most prominent differences between the two primordial populations are seen in the

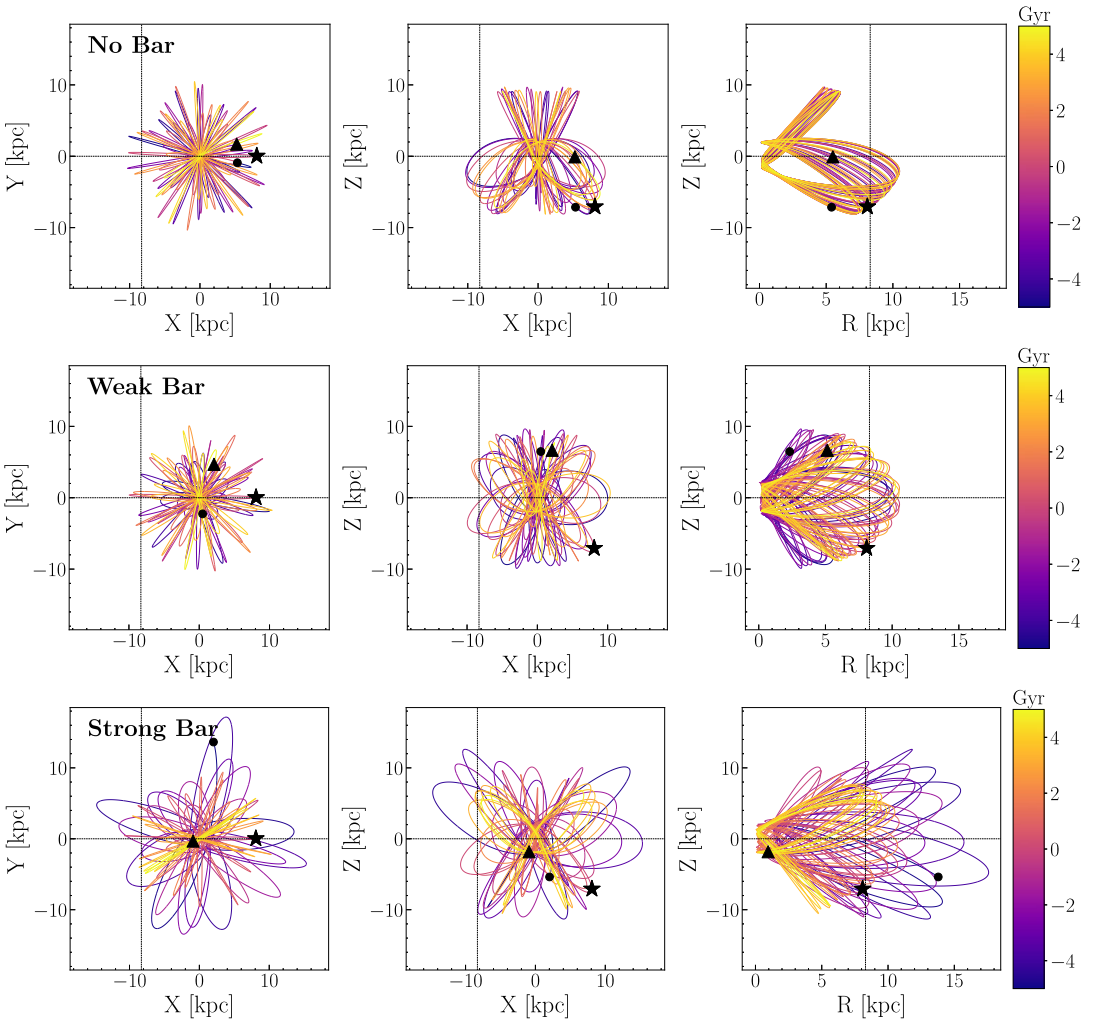

Figure 2. Example orbits for NGC 288 integrated forwards and backwards for 5 Gyr in three different potentials. The position of the cluster 5 Gyr ago is marked with a circle, the present day position is marked with a star and the position 5 Gyr in the future is marked with a triangle. The trajectory is coloured by time and presented (from left to right) in the Y-X, Z-X and Z-R planes. Top, the orbit integrated in `MWPotential2014`, middle, integrated in `MWPotential2014 + DehnenBarPotential` with weak bar characteristics, bottom integrated in `MWPotential2014 + DehnenBarPotential` with strong bar characteristics. Details of the bar characteristics are given in Section 3.1.1. The position of the sun is marked with dashed lines.

Fe-peak elements, Cr, Fe, and Co, the light *s*-process elements Y and Zr and the *r*-process elements Nd and Eu (created via neutron star mergers and magneto-rotational supernovae Côté et al. 2018; Kobayashi et al. 2020). Comparing the *s*-rich group in NGC 362 with NGC 288, reveals the same differences between elements as the *s*-weak/NGC 288 comparison, except the scale of the differences is larger overall.

To explore how chemically distinct the two GCs are relative to a GC that is not dynamically associated with the GSE, we compare our cluster abundances to the disc-like GC, NGC 6752. The bottom panel in Fig. 3 shows the absolute differences between our two GCs and NGC 6752 using the average cluster abundances (considering all the stars in NGC 362, except for the *s*-process enhanced star) and data for NGC 6752 from the differential study of Yong et al. (2013). NGC 6752 is selected for comparison as it is one of the few GCs examined using high precision differential abundance analysis (the chemically complex GC, M 22 being the only other, McKenzie et al. 2022) and has a similar metallicity to NGC 288/NGC 362 ([Fe/H] ~ -1.48, as calculated using NLTE, Kovalev et al. 2019). Additionally, we use the same reference star in Paper I as Yong et al. (2013) (mg9), therefore the two studies are anchored to the same zero-point.

We are cautious about discussing the origin of NGC 6752 as it has disc-like kinematics but is chemically complex (Yong et al. 2013). Furthermore, it has been dynamically associated with both the MW disc (implying an *in situ* origin, Massari et al. 2019) and with the *Kraken* merger event (Callingham et al. 2022). Regardless of the origin of NGC 6752, it has not yet been associated with GSE and thus we treat it as a cluster with a distinctly different origin to both NGC 288 and NGC 362. Examining the bottom panel of Fig. 3, both clusters show significantly different chemistry relative to NGC 6752 for every element in common. The largest differences between both GCs and NGC 6752 are seen in the heavier elements.

Finally, as a measure of how similar our two GCs are relative to the chemical similarities seen in *known* galactic siblings, we turn to the LMC GC system. We employ data from the two studies of Mucciarelli et al. (2010) and Mucciarelli et al. (2012) to explore the differences between a set of three similar metallicity LMC GCs (NGC 1786: [Fe/H]=−1.75, NGC 2210: [Fe/H]=−1.65 and NGC

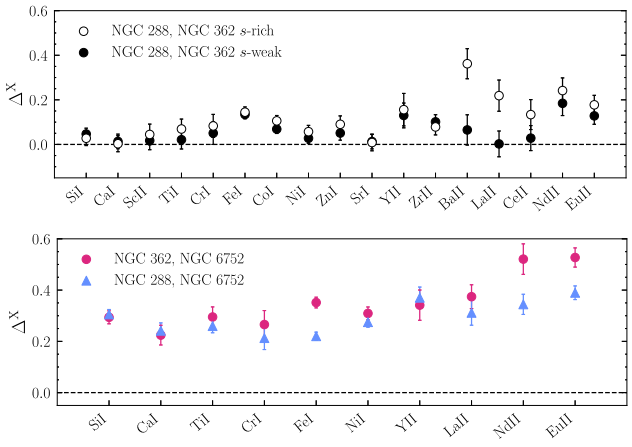

Figure 3. Comparison of the average abundance differences between NGC 288 and the two *s*-process groups in NGC 362 (top). The comparison with the *s*-weak group is shown using the filled circles, while the comparison between NGC 288 and the *s*-rich group is shown using open circles. Bottom, the differences between the two GCs in our study and the disc-like GC, NGC 6752 from Yong et al. (2013) (when considering all the stars in NGC 362, with the exception of the extremely *s*-process enhanced star NGC362-1441).

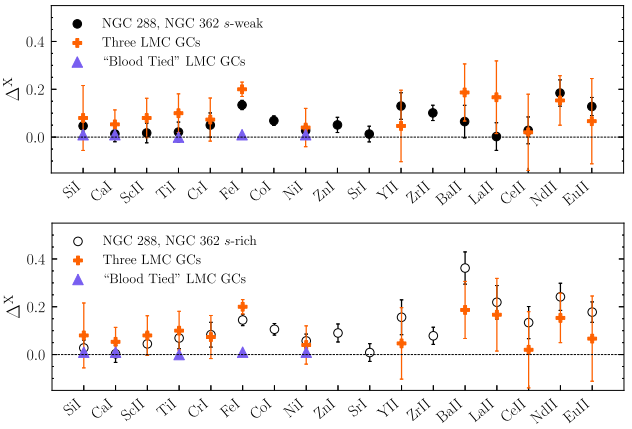

Figure 4. Comparison of the average abundance differences between NGC 288 and the two *s*-process groups in NGC 362 (top: *s*-weak, bottom: *s*-rich) to the average differences between the three LMC GCs, NGC 1786, NGC 2210 and NGC 2257 (orange) and the binary ('blood tied') LMC GCs, NGC 2136, and NGC 2137 (purple) from the studies of Mucciarelli, Origlia & Ferraro (2010) and Mucciarelli et al. (2012), respectively.

2257: [Fe/H]=−1.95) and the differences seen between the binary LMC GC system composed of NGC 2136 ([Fe/H]=−0.40) and NGC 2137 ([Fe/H]=−0.39), respectively. In the case of the binary GC system, Mucciarelli et al. (2012) suggest from the level of chemical similarity that the GCs likely formed from the fragmentation of the same molecular cloud. Both studies perform the analysis in a homogeneous way, avoiding systematic offsets introduced when combining data from independent studies.

Fig. 4 shows the average differences between each set of GCs, in each of the three studies. The intention of this comparison is to establish a benchmark for how similar GCs associated with a single parent galaxy can be.[4] Therefore, at no point do we perform a direct comparison between our MW GCs and the LMC GCs. The average abundance differences in the set of three LMC GCs are shown in orange in both panels of Fig. 4, while the differences in the two GCs with 'blood ties' are shown as the purple triangles. Note that the average abundances for the three LMCs are taken from the set of all three possible combinations. The error bars are calculated in the same way as Fig. 3

As mentioned in the previous paragraph, given that the three LMC GCs, NGC 1786, NGC 2210, and NGC 2257 are suspected siblings, their chemical similarity will inform our expectations of the sibling scenario for NGC 288 and NGC 362. The definite siblings (i.e. NGC 2136 and NGC 2137) serve as an extreme example for how similar sibling GCs can be and provide an upper limit on the level of chemical similarity between GCs. For the three LMC GC siblings we find weighted average differences in the α-elements Si, Ca, and Ti of 0.07 ± 0.02 dex, 0.12 ± 0.06 dex in the Fe-peak elements Sc, Cr, Fe, and Ni, 0.12 ± 0.07 dex in the *s*-process elements Y, Ba, La, and Ce and a difference of 0.12 ± 0.04 dex in the *r*-process elements Nd and Eu.

Comparing the three LMC GC siblings with NGC 288 and the *s*-weak group in NGC 362 (top panel of Fig. 4), one can see that our two GCs generally show greater chemical similarity than the three LMC GCs. The only exception to this is in the heavy elements Y, Nd and Eu. In the case of Nd and Eu, the two elements have a considerable contribution from the *r*-process (Nd: ∼ 43 per cent, Eu: 94 per cent, Bisterzo et al. 2011) suggesting this could be the source of the disagreement.

This exception is repeated in the lower panel of Fig. 4, where the differences between the three LMC GCs are again shown alongside the differences between NCG 288 and the *s*-rich group in NGC 362. Again, our two GCs show greater agreement across most elements except the heavy elements. In this case, our GCs show greater differences in all the elements heavier than Sr. With the exception of the disagreement in *r*-process enhancement between NGC 288 and NGC 362, the primordial populations in our GCs (NGC 362 *s*-weak) show greater agreement overall when compared to similarities seen in the three LMC sibling GCs. As expected, the LMC GC twins, NGC 2136 and NGC 2137 show the smallest disagreements.

Our second conclusion is that NGC 288 and NGC 362 display comparable, if not greater chemical similarities to those seen in the three assumed galactic siblings, the LMC GCs NGC 1786, NGC 2210 and NGC 2257. The only exception to this is in the heavy s- and r-process elements. We interpret this as support for the galactic sibling scenario.

3.2 Accretion scenario II: complete strangers

Approaching the accretion scenario for NGC 288 and NGC 362 from the other perspective, we now present primarily chemical evidence that the GCs are not galactic siblings and were not accreted together as part of the GSE event. As discussed in Section 1, this is in agreement with the findings of Myeong et al. (2018, 2019), who tentatively tag NGC 362 to the *Gaia*-Sausage accretion event. This is also in-line with the findings of Sun et al. (2023), who dissect GSE into four dynamical groups, proposing that GSE is composed of an additional three unique accretion events. They assign NGC 288 to 'GSE-b' while leaving the association of NGC 362 to the main GSE progenitor unchanged. Because the Sausage event occupies a

[4]Note that while we assume the three LMC GCs we examine are true galactic siblings which formed alongside the LMC, the LMC is proposed to host at least one accreted GC (NGC 2005, Mucciarelli et al. 2021). We avoid examining NGC 2005 for this reason.

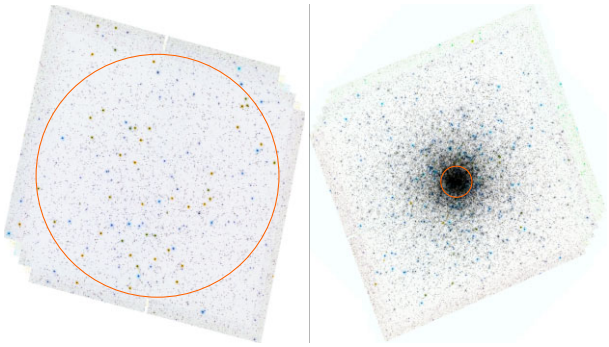

Figure 5. Snapshots from the HST HUGS Survey (Piotto et al. 2015; Nardiello et al. 2018) of NGC 288 (left) and NGC 362 (right) using the HST F275W band, the cluster core radii are marked in each image as the orange circle. The two images have similar total exposure times (NGC 288: 400s, NGC 362: 519s). Note the stark difference in the physical scale of the cluster core radii and recall that the clusters are at approximately the same heliocentric distance (∼9 kpc Baumgardt & Vasiliev 2021a). Both GCs are found near the radially solar circle and below the MW disc, placing them on halo-like orbits.

smaller region of E-L_z space, due to it's nearly net zero angular momentum, fewer GCs are declared to have a strong association. In the following sections, we discuss the intrinsic dynamical differences between the GCs, exploring potential explanations, and present the chemical distinctions between the GCs.

3.2.1 Dynamical evidence against a common origin

In the case of NGC 288 and NGC 362, one needs to do little more than look at images of the two clusters (Fig. 5) to conclude that they have either, (i) had significantly different dynamical histories or (ii) were born with very different initial conditions. Addressing the first question, as discussed in Section 3.1.1 the two GCs share many orbital characteristics in common. Despite this, they have vastly different internal characteristics. For example, the half-mass radius of NGC 288 is significantly more extended than NGC 362 (by a factor of three, Baumgardt & Hilker 2018). NGC 288 is also less massive than NGC 362 with a present day mass of 9.34×10^4 $M_\odot$ versus 2.84×10^5 $M_\odot$ (Baumgardt & Hilker 2018), resulting in a significantly lower density overall. This is readily apparent in Fig. 5, where HST images of the two clusters are shown (NGC 288 on the left and NGC 362 on the right). The core radii of the two GCs are marked with orange circles. Note that the clusters have approximately identical heliocentric distances (Baumgardt & Vasiliev 2021b).

In the following paragraphs we explore two main questions related to the dynamical histories of the clusters and the hypothesis posed at the beginning of this section. The first, is that given the upper bound on the time of accretion of the Sausage merger (10 Gyr, Fattahi et al. 2019; Gallart et al. 2019; Bonaca et al. 2020; Borre et al. 2022), could both clusters have survived to present day on their current orbits, or would they have been tidally disrupted by the MW. The second question is whether different conditions at birth could explain the present-day cluster characteristics. This question is motivated by the vastly different densities and yet nearly identical tidal radii the two clusters (as calculated according to equation (8) of Webb et al. 2013).

One way to investigate the question of cluster disruption is to look at the timescales of dynamical processes within the two clusters. Within the cluster, internal two-body relaxation coupled with external disc and bulge shocking drives a redistribution of energy. This leads to mass segregation on time-scales dependent on the magnitude of the interactions. In turn, tidal interactions with the MW gradually deplete the outer parts of the cluster resulting in a halo of potential escaping stars (Ostriker, Spitzer & Chevalier 1972; Gnedin & Ostriker 1997; Heggie & Hut 2003). Considering only two-body relaxation and under particular assumptions, the relaxation time at the half-mass radius of a GC can be estimated (Spitzer 1969; Binney & Tremaine 2008). In the case of NGC 288 ($r_{\rm hm} = 8.37$ pc), the half-mass relaxation time is 2.95 Gyr, while in NGC 362 ($r_{\rm hm} = 3.79$ pc) the relaxation time is somewhat shorter at 1.45 Gyr, reflecting the differences in cluster densities (Baumgardt & Hilker 2018).

As mentioned, in addition to two-body relaxation, disc and bulge shocking must be considered for the two GCs as they have experienced a significant number of disc passages over the last 10 Gyr. Given their present-day orbits many of these passages occurred in regions of high disc density. Disc shocking timescales can be estimated through arguments of energy injection timescales and binding energy at different points in the cluster [e.g. equation (12.9) in Heggie & Hut 2003] but is most accurately calculated via N-Body simulations. N-Body simulations of the two clusters were performed by Baumgardt et al. (2019b) who predicted the dissolution times integrating forward from present day conditions. They found a dissolution time of 10.2 Gyr for NGC 288 and 10.8 Gyr for NGC 362. Given that they are expected to survive for another ∼10 Gyr, one can conclude that they have survived for at least that long already −-answering the first question posed at the beginning of this section.

The second question posed in this section addresses the initial conditions of the clusters, could this explain how drastically different they are today? To help with our discussion, we start with an estimate of the initial cluster masses. According to Baumgardt et al. (2019b) utilizing the same simulations that determined the lifetime of the GCs, the initial cluster masses were estimated to be 4.1×10^5 $M_\odot$ (NGC 288) and 1.4×10^6 $M_\odot$ (NGC 362). Given these initial masses and the present day cluster masses (Baumgardt & Hilker 2018), both clusters have lost approximately 75 per cent of their initial mass. Note that this estimation ignores the effects of tidal shocks via interactions with giant molecular clouds during cluster formation. Therefore, they represent the initial masses post-shock phase and provide a lower limit on mass-loss.

Another interesting thing to note is that NGC 362 is proposed to be a 'post-core-collapsed' (PCC) cluster (Dalessandro et al. 2013; Libralato et al. 2018). Core collapse indicates that runaway mass segregation (driven primary by two-body relaxation) has occurred within the cluster resulting in the central density reaching a maximum. To assess the diversity of characteristics for clusters still found *in situ* around their parent galaxy, we turn to the GC system of the LMC utilizing the results of Mackey & Gilmore (2003).

Three relevant trends to our discussion are shown in Fig. 6, where the core radius, mass, and central density of LMC clusters from Mackey & Gilmore (2003) are plotted against age. Clusters that they believe are definitely PCC (and those speculated to be) are shown using the orange starred symbols in both panels. Analogues of NGC 288 and NGC 362 (sharing similar present-day characteristics) can be seen in the two panels among the oldest LMC GCs highlighted within the orange shaded regions. Three features are apparent, (i) clusters with similar ages can show a variety of core radii, (ii) only the most massive of the ancient LMC clusters have survived to present day, and (iii) the central density of the surviving GCs spans a large range of values

This suggests that clusters born in the same system can survive to the present day *and* display significantly different internal characteristics (assuming they all formed *in situ*, unlike the proposed

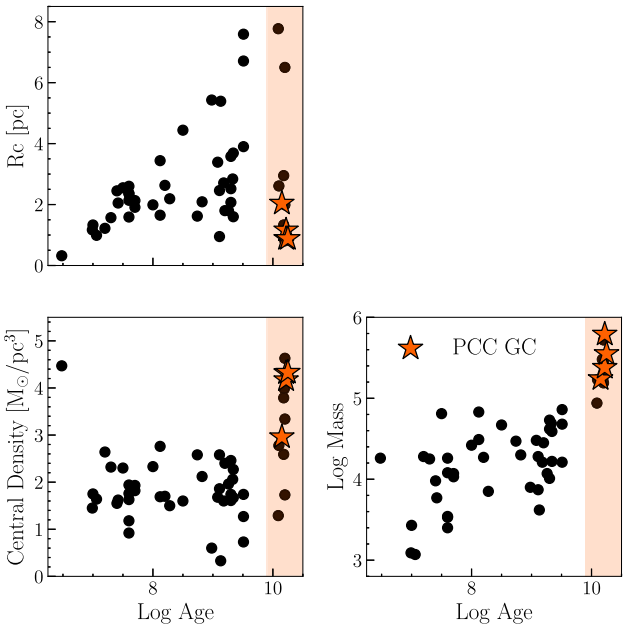

Figure 6. Core radii (top), log mass (bottom left) and central density (bottom right) as functions of age for LMC GCs from Mackey & Gilmore (2003). Proposed PCC clusters are shown as the orange stars. The orange shaded region marks the area where NGC 288 and NCG 362 would occupy given their ages, and initial and present day masses. Note that both PCC and non-PCC clusters are found in this region.

scenario for NGC 2005, Mucciarelli et al. 2021). This conclusion is supported both by simulations of GC formation like those of McKenzie & Bekki (2021) who saw physically diverse GCs form with similar metallicites and by *N*-body simulations that reconstruct the initial cluster masses (e.g. Baumgardt & Hilker 2018).

To further validate this idea, we explored the distribution of GC core radii as a function of radial distances from the optical centre of the LMC. Among the oldest clusters, both PCC and non-PCC GCs were found at similar radial distances. Although this is only a snapshot of the cluster orbits and may not be indicative of the average radial distances, it does reinforce the idea that clusters at similar locations within a galaxy can show very different internal characteristics. Given both the initial and present day masses of both NGC 362 and NGC 288 and recent estimates of their ages (∼11 Gyr, VandenBerg et al. 2013), both clusters would be coincident with the clump of GCs shown in the upper right corner of the right panel in Fig. 6, suggesting that at least in the environment of the LMC they would have survived until present day.

Our third conclusion is that there is no strong dynamical evidence against a common origin for the two clusters. The drastically different present-day characteristics of NGC 288 and NGC 362 can be explained if they formed with significantly different initial conditions. This is supported by the diversity of ancient clusters within the LMC.

3.2.2 Chemical evidence against a common origin

To explore the chemical differences between the two clusters that could exclude the sibling scenario, we compare the average cluster abundances with trends found in GSE and Sausage stars. In this comparison, if either NGC 288 or NGC 362 is found to be chemically distinct from the GSE, then this provides evidence against the common origin hypothesis. A comparison is possible thanks to the numerous studies examining the chemistry of GSE and Sausage stars (see Section 1). Two recent studies by Matsuno et al. (2021) and Aguado et al. (2021) have published dedicated high precision chemistry of stars tagged to the two proposed accretion scenarios.

Fig. 3 reveals that both *s*-process populations in NGC 362 show similar disagreement in the abundance of Eu when compared to the average value in NGC 288. The other element that shows the largest disagreement between the *s*-rich population and NGC 288 is Ba. Given the dominance of the *s*- and *r*-process production pathways for Ba and Eu, respectively (Bisterzo et al. 2011), we select these two elements to act as characteristic elements representative of their nucleosynthetic groups and choose to compare the two with measured GSE and Sausage abundances.

Ba abundances in local group dGals vary, with some dGals showing Ba-enhancement relative to MW field stars at the same metallicity (e.g. Fornax Shetrone et al. 2003; Tolstoy, Hill & Tosi 2009; Letarte et al. 2010; Lemasle et al. 2014), while others show MW-like Ba abundances (e.g. Sculptor Shetrone et al. 2003; Tolstoy et al. 2009; Hill et al. 2019; Skúladóttir et al. 2019a). Unfortunately, both Sausage and GSE stars appear to occupy the latter distribution (Monty et al. 2020; Aguado et al. 2021; Matsuno et al. 2021), making [Ba/Fe] alone an uninformative discriminator of galaxy membership in this case.

The ratio of Ba to Eu serves as a diagnostic of the relative contributions of $s-$ and *r*-processes within systems, with dGals ratios favouring *r*-process dominance at early times (Tolstoy et al. 2009, and references therein). Both Ba and Eu abundances were measured in GSE (Matsuno et al. 2021) and Sausage stars (Aguado et al. 2021) using data from the GALAH Survey ($R \sim 28,000$, Buder et al. 2021) and observations from VLT/UVES, respectively. Both studies found that the [Ba/Eu] abundance ratios in their stars pointed to a strong dominance in *r*-process sources due to an enhancement in Eu. This was also hinted at earlier in the study of Yuan et al. (2020), where they recovered two known Eu-enhanced stars ([Eu/Fe]>+1) in GSE through dynamical tagging.

We find this is also the case in NGC 288 and NGC 362 where we detect a marginal *r*-process enhancement relative to *s*-process, with negative [Ba/Eu] values in both clusters (in the case of the primordial *s*-weak group in NGC 362). Average differential ratios of Ba to Eu compared to the average measurement error (adding the measurement errors of Ba and Eu in quadrature) were found to be $\Delta^{\mathrm{Ba/Eu}} = -0.10 \pm 0.04$ in NGC 288 and $\Delta^{\mathrm{Ba/Eu}} = -0.16 \pm 0.07$ in the *s*-weak group. Recall that $\Delta^{\mathrm{X/Y}}$ in this case refers to the differential abundances for the two clusters derived in Paper I. When considering all the *s*-process elements with multiple line measurements (Y, Ba, Ce and La) versus the *r*-process element Eu, the average ratio of *s*/*r* in NGC 288 is -0.05 ± 0.04 dex and -0.19 ± 0.05 dex in the *s*-weak group in NGC 362.

The greatest *s*/*r* deficit in each cluster or group, was found in Ba in NGC 288 ($\Delta^{\mathrm{Ba/Eu}} = -0.10 \pm 0.04$) and in Y in both *s*-process groups NGC 362 ($\Delta^{\mathrm{Y/Eu}} = -0.26 \pm 0.05$ in the *s*-weak group.) Additionally, the average differential Eu abundances in the both clusters is elevated, with NGC 362 showing greater Eu-enhancement than NGC 288 by ∼0.15 dex. Note that the Eu-enhancement does not change between groups in NGC 362, leading to the conclusion in Paper I that the enhancement in the *r*-process element is primordial.

Another useful ratio to explore is [Eu/Mg] which is sensitive to the delay time of neutron star mergers in the production of Eu. Matsuno et al. (2021) found that [Eu/Mg] appeared significantly higher in GSE stars when compared to a population of *in situ* MW stars ([Eu/Mg] ∼0.40 dex in GSE stars versus [Eu/Mg] ∼0.20 dex in

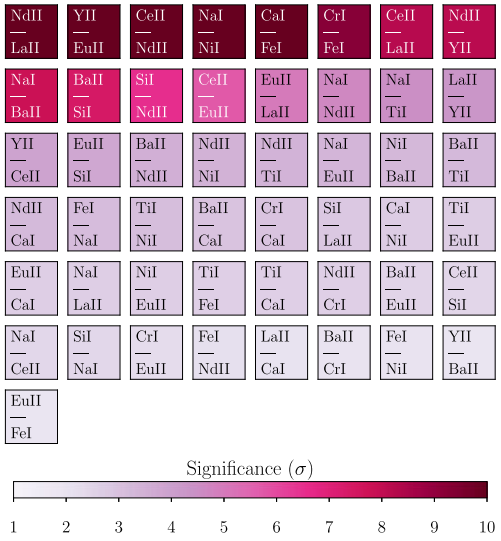

Figure 7. All possible well-measured element ratios coloured by how significantly different they are between the primordial *s*-weak group in NGC 362 and NGC 288. Only elements with more than one line are considered (with the exception of Eu are shown). Note the differences in the ratio of the first peak *s*-process element Y and the *r*-process element Eu between the clusters.

in situ stars at [Fe/H] ~ -1.3 dex). Although we do not consider Mg to be one of the best-measured elements in our study, we consider the cluster abundances of [Eu/Mg]. Both groups in NGC 362 show higher $\Delta^{\mathrm{Eu/Mg}}$ abundance ratios than NGC 288, with an average difference of $\Delta^{\mathrm{Eu/Mg}} = 0.27 \pm 0.07$ in the *s*-weak group compared to $\Delta^{\mathrm{Eu/Mg}} = 0.19 \pm 0.11$ in NGC 288. The ratio of [Eu/Mg] in both groups in NGC 362 place the cluster between average GSE and *in situ* MW values, while NGC 288 falls directly on-top of the average *in situ* ratio.

Choosing a more reliable α-element tracer in our study, namely Si, we see the same but more marked difference between the two clusters ($\Delta^{\mathrm{Eu/Si}} = 0.27 \pm 0.04$ in the NGC 362 *s*-weak group and $\Delta^{\mathrm{Eu/Si}} = 0.09 \pm 0.03$ in NGC 288). NGC 362 shows on average a $\sim$0.2 dex higher [Eu/Si] abundance ratio compared to NGC 288.

To confirm the difference in [Eu/α] ratios between the two clusters, we cross-matched the catalogues of Vasiliev & Baumgardt (2021) and GALAH DR3 (Buder et al. 2021) to select high probability cluster members from our two GCs within GALAH. The catalogues were then further refined by setting the DR3 flag `S/N_c3_iraf` > 30. In total we considered 23 stars in NGC 362 and 76 in NGC 288. The average values of [Eu/Si] in the cleaned NGC 362 and NGC 288 catalogues were 0.50 and 0.26 dex respectively. NGC 288 showed a larger spread in [Eu/Si] than NGC 362, with σ of 0.2 dex versus 0.1 dex in NGC 362 for a similar number of stars and range in metallicity. The difference in [Eu/Mg] between the two clusters is less clear in GALAH, but NGC 362 still displays a higher abundance ratio overall.

Neglecting a potential association with GSE, we also delve deeper into the abundance differences between the two clusters, comparing the primordial *s*-weak group in NGC 362 to all stars in NGC 288. The results of this are presented in Fig. 7 where all possible well-measured element ratios are compared between the *s*-weak group in NGC 362 and all stars in NGC 288. Each ratio is coloured by the significance, quantified as the ratio of the absolute difference between clusters over the uncertainty in the difference, only the elements with more than one line are considered (with the exception of Eu). Fig. A1 shows the significance of the differences between all possible element ratios.

The first interesting difference in ratios we note is the ratio of Y to Eu, followed further down by the ratio of Y to Nd. These two ratios represent two measurements of the ratio of an *s*-process to *r*-process element in the clusters (Nd being both *s* and *r*). This is in-line with the findings of Section 3.1.2, where the clusters show sibling-level similarities, with the exception of the heavy elements. Interestingly, the ratios of Ba to Eu are not significantly different, but the ratios of Zr to Nd (shown in Fig. A1) are. This could imply that the first *s*-peak elements, produced both by AGB and through core collapse supernovae (CCSNe), show greater distinctness between clusters versus the AGB-dominated *s*-process elements like Ba (Hansen, Montes & Arcones 2014; Kobayashi et al. 2020). In all cases, the ratios are significantly more negative ($\sim$0.2 dex) in NGC 362, further supporting the dominance of *r*-process production in the cluster.

Our fourth conclusion is that the abundance of Eu and ratio of [Eu/Si(Mg)] in the primordial s-weak group in NGC 362 more closely resembles Sausage and GSE stars at the same metallicity than NGC 288. Furthermore, distinct chemical differences are found between the two clusters, primarily in the ratios of the first peak s-process to r-process elements, with the r-process in NGC 362 showing clearer dominance.

4 FITTING NUCLEOSYNTHETIC GROUP RATIOS USING A GALACTIC CHEMICAL EVOLUTION MODEL

To explore the chemical abundance histories of the host galaxy(ies) around which NGC 288 and NGC 362 formed, we now experiment with replicating the trends in both clusters using a galactic chemical evolution (GCE) model. This assumes the GC chemical abundances will reflect those of their host galaxy at the time of cluster formation. We accept this assumption as we are not investigating GCE models with the intention of deriving the dGal chemical evolution history. Instead, our aim is to explore whether the abundance ratios found in NGC 362 and NGC 288 can be explained using a single model and whether this model is consistent with GSE, the proposed host galaxy.

To support this assumption we reference several studies, the first being the study of Koch-Hansen, Hansen & McWilliam (2021), where the GSE-tagged GC NGC 1261 (tentatively tagged to the Sausage) was used to infer the *r*-process enrichment of GSE. This was done after confirming several abundance ratios in common between the GC and GSE stars. In their study of the LMC GC NGC 1718, Sakari, McWilliam & Wallerstein (2017) also recovered GC abundances consistent with LMC field stars. McWilliam, Wallerstein & Mottini (2013) found the same in the Sagittarius dGal, where Sagittarius field stars and tagged GCs showed consistent chemistry, particularly in α-elements abundances. Further afield, the Fornax dGal GC H4 was also found to show chemical consistency with Fornax field stars in α-abundances and clear chemical distinction from MW halo stars (Hendricks et al. 2016). Finally, in their study of chemical abundances in 15 LMC GCs derived from integrated light spectroscopy, Chilingarian & Asa'd (2018) showed that the chemical evolution history of the LMC built using the GC abundances alone agreed with the history derived using resolved spectra of individual LMC stars.

4.1 The galactic chemical evolution model

We create our GCE model of GSE from the 'baseline' model (Model A) of Matsuno et al. (2021, discussed in Section 4 of their

paper), which was created to both replicate and predict the chemical abundance ratios found in accreted GSE stars. To build our GCE we use the OMEGA module (Côté et al. 2017) within the NuPyCEE framework (Ritter et al. 2018a). OMEGA utilizes both the NuGrid stellar evolution models (Pignatari et al. 2016; Ritter et al. 2018c) and the SYGMA module (Ritter et al. 2018b) to derive chemical yields associated with evolving simple stellar populations. We choose a closed-box model, primarily for simplicity and to avoid exploring galactic physics (i.e. in-flows and out-flows), which Côté et al. (2017) found are not well-constrained when fitting a small number of abundance ratios.

As a first step, we adopt approximately the same initial gas mass (2.5×10^9 $M_\odot$), the same final stellar mass (1×10^9 $M_\odot$) and the same total integration time (3 Gyr) as Matsuno et al. (2021) to build our model. Like Matsuno et al. (2021), we also adopt a Chabrier IMF (Chabrier 2003) with a lower mass bound of 0.1 $M_\odot$ and an upper bound of 100 $M_\odot$, adopt a power-law ($\beta - 1$) for our SNIa delay time distribution[5] and assume an initial neutron star merger (NSM) rate efficiency of 0.5 per cent for stars in the mass range $8\ M_\odot < M < 20\ M_\odot$. Our baseline model differs from Matsuno et al. (2021) in that we apply mostly different yield tables and allow for the production of the Eu via multiple sources. For our AGB and massive star yields we make use of the yield table provided by OMEGA, which adopts yields from the MESA models only (Paxton et al. 2011) and fixes the electron fraction within neutron stars at $Y_e = 0.4982$ following the prescription of Young et al. (2006). For the SNIa yields, we adopt the same yields as Matsuno et al. (2021), that of Seitenzahl et al. (2013), using the table provided by OMEGA created to include a mixture of stable and unstable isotopic yields. Finally, we adopt the neutron star merger *r*-process yields of Rosswog et al. (2014).

As discussed in Matsuno et al. (2021), their baseline GCE model is selected to explore the high [Eu/Mg] abundance ratios they observed in GSE stars in GALAH. To explain the elevated ratio (relative to MW field stars), they explore two possible explanations. The first is that Eu is overproduced in GSE due to a combination of a delayed production of *r*-process elements and prolonged SF history. The second is that Mg is underproduced as a result of a top-light IMF (manifesting as less massive CCSNe and a decreased enrichment in Mg). Ultimately, their findings support the first scenario, that the overabundance of Eu is best explained by an excess of NSMs. This is broadly in agreement with previous work that suggests NSMs are the primary site of Eu production (Ji et al. 2016; Côté et al. 2018).

Matsuno et al. (2021) also discuss the implications of NSMs being the primary *r*-process site in GSE in the context of enrichment timescales and NSM delay times. Because GSE is a disrupted dGal, the time of accretion or disruption by the MW places a constraint on the end of SF within the dGal. As discussed in Section 3.2.1, estimates for the time of GSE-MW merger place an upper bound of 10 Gyr ago (although it is hard to define when exactly accretion occurs and if this is coincident with the halting of SF). Unlike GSE, to explain the *r*-process enrichment patterns in the MW and surviving satellites, a secondary *r*-process enrichment site (in addition to NSMs) has been suggested (Côté et al. 2019; Skúladóttir et al. 2019b; Kobayashi et al. 2020; Skúladóttir & Salvadori 2020).

The necessity of a secondary formation site within the MW stems from the need to explain *r*-process enrichment at all times, coupled with the predicted delay time for NSMs. Estimates for the delay time range from 50 Myr to 4 Gyr when galactic chemical enrichment histories are used to place the constraints (Côté et al. 2018; Skúladóttir & Salvadori 2020; Naidu et al. 2022; de los Reyes et al. 2022), to ∼7−4 Gyr from host galaxy follow-up of the confirmed NSM, GW170817 (Blanchard et al. 2017). Assuming SF stopped in GSE ∼10 Gyr ago, the delay time for NSMs within the dGal is necessarily closer in agreement to the shorter delay times. While Matsuno et al. (2021) adopt a delay time of 20 Myr, Naidu et al. (2022) derive a minimum delay time of 500 Myr from additional spectroscopy of GSE stars, suggesting that rare CCSNe could explain some of the earliest enrichment in GSE and offering another *r*-process production site within the dGal.

[5]The delay time distribution captures the rate of events as a function of time following a burst of SF.

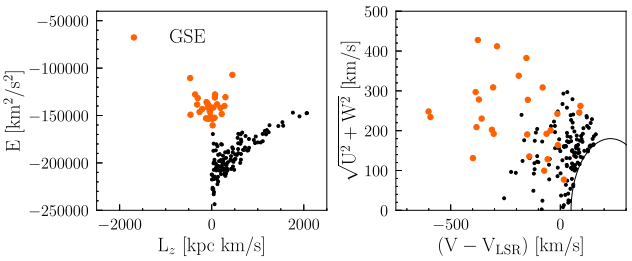

Figure 8. Selections of GSE stars from GALAH DR3 following several chemical, kinematic, and dynamical cuts. The GSE selection is presented in orange, while a selection of *in situ* stars is shown in black. The samples are shown in energy versus z-angular momentum (left) and in the classical Toomre diagram (right). All orbital parameters are determined assuming a McMillan17 potential in galpy.

4.2 Replicating the chemical trends seen in both *Gaia*-Sausage-Enceladus stars and our clusters

To test our baseline GCE model, we selected a representative element from four nucleosynthetic groups (discussed in-depth in Paper I). To select each representative element, we considered both the quality of the abundance measurements and the contribution of each nucleosynthetic process to the production of that element (Bisterzo et al. 2011; Kobayashi et al. 2020). We chose Si to represent the α-elements, Fe the Fe-peak elements and Ba and Eu to represent *s*- and *r*-process elements, respectively. The quality of the fit between observations and model predictions for each of the six unique ratios was then assessed.

To aid in assessing the quality of the GCE model, we (i) selected the ratio of Eu to Si to act as the primary discriminator, based on the discussion presented in Section 3.2.2 and (ii) selected a sample of GSE stars from GALAH DR3 to better assess the quality of the fit. To select the GALAH GSE stars, we selected stars from Table 5 of Buder et al. (2022) and applied the following cuts:

(i) probability_chemical_selection $\geq$0.45
(ii) probability_dynamical_selection =1

Further cuts in the quality of the data (flags), kinematic and dynamical constraints were taken directly from Section 2 of Matsuno et al. (2021) and applied to the GSE population. All kinematic (UVW) and dynamical parameters (J_r, E, and L_z) were determined assuming the McMillan17 potential in galpy as in Matsuno et al. (2021), integrating for 1 Gyr. The GSE sample was then further cleaned to only include giants with stellar parameters in the same range as our program stars ($T_{eff} \in [3800, 4400]$ K, $\log g \in [0.2, 1.2]$ cm/s^2). The final sample selection of GSE stars is presented in Fig. 8 showing

the dynamical footprint of the sample in E versus L_z space and in a classical Toomre diagram. In the diagram, we adopt $v_{LSR} = 229$ km/s (Eilers et al. 2019).

Finally, as further verification of the GCE model, we used the Gaussian Mixture Model (GMM) of Myeong et al. (2022) to construct predictions for the mean GSE abundances in our six abundance ratios. In their study, Myeong et al. (2022) fit four distinct components to the MW halo within their model, GSE being the only accreted component. Because the GMM predictions for GSE occur at higher metallicities than our two GCs, we extended the predictions using linear fits. This was done using the angle between the semi-minor and semi-major axes of the covariance ellipse associated with GSE probability distribution functions. In the case of [*s*/*r*] the covariance ellipse is nearly circular and so the direction of the trend is highly uncertain. We consider the predictions from both the physically motivated (and tuneable) GCE model and the data-driven GMM to be complementary given the diversity of the two approaches. However, we acknowledge that the two approaches are not completely independent as GALAH data is used to some extent in both approaches to constrain the final model.

To evaluate the baseline model and explore alternate solutions, we collapsed our two GCs (the two *s*-process groups in NGC 362, NGC 288) and the GALAH GSE data set into their average values with error bars denoting the intrinsic spread (standard deviation). The baseline model was then fit to the average ratio values over a metallicity range centred around GC averages ($-1.5 <$ [Fe/H] < -1.2 dex), in the six different combinations. Initial evaluation of the baseline model found that model failed to reproduce the ratio of [Eu/Si] associated with both the GSE data points and GMM trends, underpredicting both. The only ratios in which the baseline model fit the GSE data points well was in [Fe/Eu], [Ba/Eu] and [Fe/Ba], suggesting the *s*- and Fe-peak elements were well-reproduced with the baseline model −-but not the *r*-process abundances.

Given the failure of the baseline model to fit the GSE [Eu/Si] ratio (our primary discriminator), we decided to explore increasing the production of Eu in our models through varying two different parameters. The first parameter was the fraction of NSMs in the mass range $8\ M_\odot < M < 20\ M_\odot$, and the second was the transition mass from AGB to massive stars (the minimum mass for a CCSNe). Both should primarily effect the α, *s*-, and *r*-process channels. The remaining galaxy characteristics including the closed box assumption, yield tables, and integration time remain unchanged as described in Section 4.1

Because our aim was not to derive the GCE model for our two GCs, simply to explore how well a GCE model designed for GSE fits the data, we refrained from a full exploration of parameter space to derive a best-fit GCE model. Instead, we chose to simply modify the baseline model, exploring only transition masses (M_T) in the range $8M_\odot < M < 12M_\odot$ and to gradually increase the NSM fraction (f_{NSM}). This resulted in three more GCE models in addition to the baseline model, models 2, 3, and 4 with details provided in Table 2. From the predictions given for the three additional models, and considering our choice of emphasis on the fit to [Eu/Si], we found Model3 best-fit the GSE stars at higher metallicities (near that of NGC 362) and Model4 to best-fit the lower metallicities (near that of NGC 288). As listed in Table 2, both Models 3 and 4 have a higher fraction of NSMs compared to the baseline model (0.25 per cent and 0.5 per cent, respectively) and a higher turnover mass marking the change from AGB to massive star yields (10 and 12 $M_\odot$, respectively). The predictions from the two models are shown in Fig. 9. Model3 is shown using the solid black line and Model 4 the dashed line.

Table 2. Galactic chemical evolution models of GSE created to explore fitting the abundance ratios found in our GCs. Each model is characterized by the two parameters we chose to tune; the transition mass from AGB to massive stars (M_T) and the fraction of NSMs for stars in the mass range $8\ M_\odot < M < 12\ M_\odot$. Further details of the models are given in the text in Section 4.1. Predictions for the best-fit models, Models 3 and 4 in the six abundance ratios are shown in Fig.s 9.

Name	M_T [$M_\odot$]	f_{NSM}
Model1 (Baseline)	8	0.005
Model2	10	0.0075
Model3	12	0.0075
Model4	12	0.010

4.3 Evaluating the *Gaia*-Sausage-Enceladus model fits to our globular clusters

Regarding the fit to our GCs presented in Fig. 9, without considering the GCE models themselves, both groups in NGC 362 appear more similar to the average GALAH GSE abundances at the same metallicity. In fact, complete overlap is seen between the GALAH GSE average and one or both groups in NGC 362 in all six ratios. This was discussed to some extent already in Section 3.2.2. Also, one or both groups in NGC 362 appear within 2σ of the GMM predictions in every ratio, while this is only true for NGC 288 in four of the six ratios. Naturally, this results in the GCE models better fitting the average abundance ratios in NGC 362 overall versus NGC 288. This is especially apparent in the ratios of [s/α] and [r/α]. Note that the apparent disagreement between the GMM and GALAH data points in these ratios is likely due to different samples of GALAH GSE stars being selected by our study and that of Myeong et al. (2022).

Interestingly, Model3 with the lower fraction of NSMs and closer to the baseline model, better reproduces the abundances of both groups in NGC 362 than it does GSE. The abundance ratios in NGC 288 cannot be easily reproduced with a single model and instead vary between the models 3 and 4 depending on the ratio. In the case of the *s*-/*r*-process abundance ratio, both models predict the same ratio and are able to reproduce the ratio found in all groups equally. Finally, if we use the predicted elemental dispersion in the GSE GMM (the shaded regions in Fig. 9) as a proxy for the chemical (in-)homogeneity in the GSE progenitor, we can see that the disagreements between NGC 288 and GSE stars cannot be explained by chemical in-homogeneity alone. That is, if the GCs are truly siblings, this demands a degree of chemical in-homogeneity in the GSE progenitor that is larger than what is presently predicted by the GMM.

Our fifth, and final conclusion, is that the abundance ratios in NGC 362 are well reproduced by a slightly modified GCE representative of GSE. It is unclear whether this is true in NGC 288. This supports a scenario in which the GCs are not siblings, or demands a greater degree of chemical in-homogeneity in the GSE progenitor than what is presently seen in the data.

5 SUMMARY

Using data from our recent differential chemical abundance study of the MW GCs NGC 288 and NGC 362 (Monty et al. 2023, Paper I), we explored the chemo-dynamical likelihood that the two GCs are galactic siblings. The two GCs exhibit similar metallicites ($[Fe/H]_{ave} = -1.44$ in NGC 288 and $[Fe/H]_{ave} = -1.30$ in NGC 362 from Paper I) and nearly identical orbits ($r_{peri} = 0.25$ pc, $r_{apo} = 10.90$ pc, $e = 0.96$ in the case of NGC 288 and $r_{peri} = 0.38$ pc, $r_{apo} =$

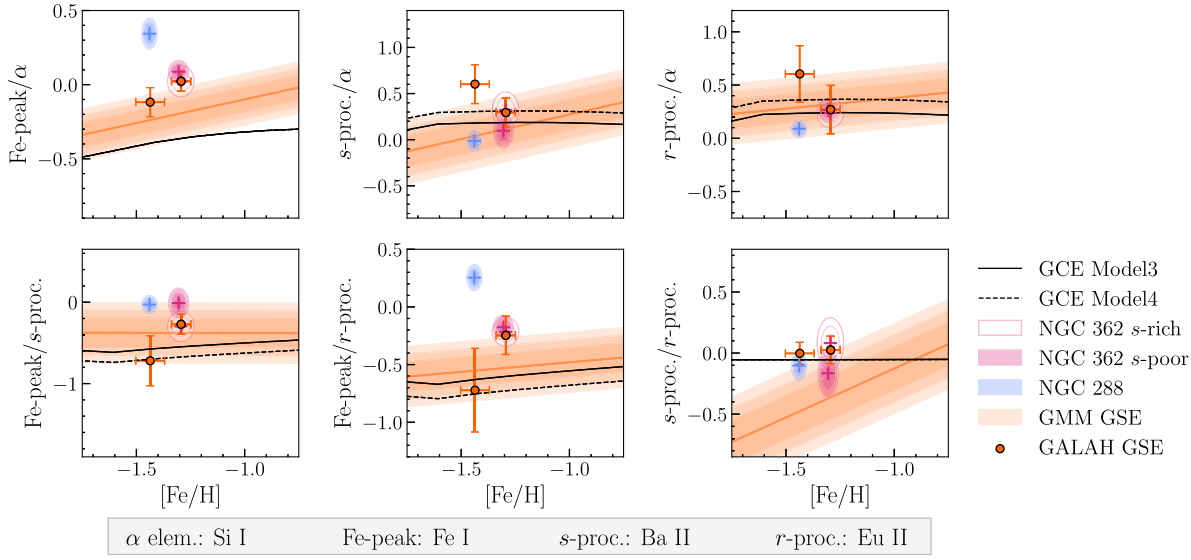

Figure 9. Predictions for the abundance ratios of four different nuclosynthetic channels (as characterized by the elements included in the key below the figure) from the two best-fit galactic chemical evolution models discussed in Section 4.2. Model parameters are given in Table 2 and discussed in Section 4.1. Average values for our two *s*-process groups in NGC 362, and a subset of GSE stars from GALAH are shown for each ratio. Trends for GSE predicted from the GMM of Myeong et al. (2022) are shown as the orange shaded regions marking the 1σ, 1.5σ and 2σ deviations from the predicted trends. Note that the GCE models are overlapping in the panel showing the prediction for the ratio of Fe-peak/α and *s*/*r*.

13.17 pc, $e = 0.94$ in NGC 362). Thus far only the position on the MW GC age-metallicity relation and/or the integrals of motion have been used to either infer or refute siblinghood for the two GCs (Myeong et al. 2018; Massari et al. 2019; Myeong et al. 2019; Callingham et al. 2022; Malhan et al. 2022). Both GCs are proposed to have been brought in as part of *Gaia*-Enceladus merger (Helmi et al. 2018; Massari et al. 2019), while only NGC 362 has been tagged to the *Gaia*-Sausage (Belokurov et al. 2018; Myeong et al. 2018, 2019). As part of our exploration, we assessed chemical and dynamical evidence both *for* and *against* the galactic sibling scenario.

To support the galactic sibling scenario, we integrated the two GC orbits in a static MW-like potential which – contrary to all previous tagging studies of these GCs – contained a representation of the MW bar. We explored two different models of the bar. The first model was represented using the Dehnen Potential, as implemented in the PYTHON-based galactic dynamics package `galpy` (Dehnen 2000; Bovy 2015). The second was built using Ferrers Potential (also as implemented in `galpy`) which represented both the bar and the MW bulge. Both weak and strong models of the bar (as quantified by the bar strength, A_f) were explored and each GC was integrated for 5 Gyr. In the case of integration in the presence of both a weak and strong bar, no major changes to the two cluster orbits were found. The *z*-component of the angular momentum in the two clusters was found to change by no more than ∼40 km/s kpc in NGC 288 and no more than ∼20 km/s kpc in NGC 362. In both cases, the clusters retained their associated with *Gaia*-Enceladus as defined by Massari et al. (2019).

To provide chemical support for the sibling scenario we, (i) explored the chemical similarities between the two GCs, (ii) compared each to the disc-like GC NGC 6752, and (iii) compared differences between NGC 288 and NGC 362 with the differences seen in the three LMC GCs NGC 1786, NGC 2210 and NGC 2257 as well as the LMC 'blood tied' GCs, NGC 2136 and NGC 2137. To compare our two GCs, we first split NGC 362 into two groups separated by average *s*-process abundance, following the discovery and designation made in Paper I. In Paper I, the *s*-weak group was found to be older than the *s*-rich group and to share greater chemical similarities with NGC 288. Therefore, we compared the *s*-weak group and NGC 288 to probe the primordial chemical similarities between the two GCs.

Overall, we found a maximum disagreement of no more than ∼0.2 dex between the *s*-weak group in NGC 362 and NGC 288. The largest disagreement occurred in Nd (an element with both *s* and *r* process contributions.) Comparing the *s*-rich group with NGC 288 showed larger disagreement (>0.2 dex) with the heavy elements (heavier than Y) but small disagreements otherwise. Both GCs showed large differences in every element when compared to NGC 6752 (using data from the study of Yong et al. 2013). When comparing differences between the LMC siblings using data from Mucciarelli et al. (2010), to the differences between the *s*-weak group and NGC 288, the *s*-weak group and NGC 288 showed equivalent or greater chemical similarity across nine of the thirteen (9/13) elements in common between studies. However, both groups in NGC 362 showed larger disagreement with NGC 288 in *r*-process abundances compared to those seen in the three LMC siblings. In the case of the comparison between the *s*-rich group in NGC 362 and NGC 288, all of the heavy element abundances showed larger disagreements compared to those seen in the LMC siblings.

Dynamical evidence against the sibling scenario centred primarily around an investigation into the different apparent dynamical states of the two. Specifically, that NGC 362 is a suspected post-core-collapse (PCC) GC while NGC 288 is not (Harris 1996). Characteristics of LMC GCs from the study of Mackey & Gilmore (2003) were used to explore the relationships between mass, age, radial distance from the LMC centre and cluster core collapse. PCC GCs in the LMC were among the oldest and most massive GCs, supporting the idea that they are among the most dynamically evolved. However, non-PCC clusters were also observed among the oldest LMC GCs, suggesting that GCs could survive to present day without significant dynamical evolution under the assumption of differing initial conditions (mass, density and stellar populations). Therefore, we suggest that

significantly different initial conditions are required to explain the near-identical orbits but vastly different dynamical stars of NGC 288 and NGC 362. This is supported by existing *N*-body simulations of the clusters (Baumgardt & Hilker 2018).

Chemical evidence against the sibling scenario stemmed mainly from further exploring the disagreement in heavy elements discovered in Section 3.1.2. This involved comparing with the chemical abundances of GSE stars from the studies of Matsuno et al. (2021) and Aguado et al. (2021), who studied *Gaia*-Enceladus and *Gaia*-Sausage stars, respectively. Given that *Gaia*-Enceladus includes the entirety of *Gaia*-Sausage stars, we refer to both as 'GSE', as is common in the literature. GSE stars were found to be enhanced in the *r*-process element Eu and dominated overall by the *r*- compared to the *s*-process. The primordial, *s*-weak population in NGC 362 was found to be more strongly dominated by the *r*-process than NGC 288 (with a maximum difference of $\Delta^{\mathrm{Y/Eu}} = -0.26$, compared to $\Delta^{\mathrm{Ba/Eu}} = -0.10$ in NGC 288). The ratio of *r*-process to α elements was also used to explore an association with GSE, following the discovery by Matsuno et al. (2021) that GSE stars show an enhancement in [Eu/Mg] ([Eu/Mg] $\sim$0.40 dex in GSE stars versus [Eu/Mg] $\sim$0.20 dex in *in situ* stars at [Fe/H] ~ -1.3 dex). We found that both groups in NGC 362 showed a higher ratio of $\Delta^{\mathrm{Eu/Mg}}$ overall, with an average enhancement of $\sim$0.1 dex relative to NGC 288. When considering the better measured α-element, Si, the average value of $\Delta^{\mathrm{Eu/Si}} = 0.27$ in the *s*-weak group and $\Delta^{\mathrm{Eu/Si}} = 0.09$ in NGC 288.

To confirm these differences, stars from the two clusters were recovered in the GALAH DR3 catalogue (Buder et al. 2021), with the GALAH abundances confirming that NGC 362 was enhanced in both ratios relative to NGC 288. Overall, NGC 362 showed greater agreement with GSE stars when considering trends in the ratios of *s*-, *r*-, and α elements. Finally, when comparing the *s*-weak group in NGC 362 directly to NGC 288, the two showed a marked difference in the ratio of first peak *s*-process elements (primarily in Y) to *r*-process elements (Eu), suggesting primordial differences between the two clusters.

Finally, we experimented with fitting the chemical abundance ratios in the two GCs with a galactic chemical evolution (GCE) model. The model was created under a closed-box assumption using the PYTHON chemical evolution package `OMEGA` (Côté et al. 2017). We adopted as our base model, the GCE model of Matsuno et al. (2021) and explored the fit to six different element ratios representing the combination of four different nucleosynthetic groups (α: Si I, Fe-peak: Fe I, *s*-: Ba II and *r*-process: Eu II). A selection of GSE stars were also selected from the study of Buder et al. (2022) and the GMM predictions from the study of Myeong et al. (2022) were also used to help evaluate the fit of the GCE model. In almost all element ratios, one or both *s*-process groups in NGC 362 showed excellent agreement with the GALAH GSE star averages. In the case of s/α and r/α, the two were overlapping. NGC 288 showed less agreement overall, with the closest agreement being in the ratio of s/r where the two showed a difference of $\sim$0.1 dex.

The base GCE model was found to under-produce in the *r*-process element Eu relative to the α element Si leading to the exploration of three additional models to improve the fit. Overall, the best-fit GCE model to the GALAH GSE datapoints was found to be Model 3 at higher metallicities (NGC 362-like) and Model 4 at lower (NGC 288-like) metallicities. Models 3 and 4 saw the fraction of neutron star mergers increase by 0.25 per cent and 0.5 per cent and the turnover mass from AGB to massive stars increase by two and four solar masses respectively from the baseline model. Model 3 was found to fit primordial *s*-weak group in NGC 362 remarkably well in the ratio of [r/α] and [s/α].

6 CONCLUSIONS

In conclusion, although the clusters show remarkable chemical similarities and appear dynamically coincident to the GSE merger in integrals of motion space, they show distinct differences in *r*-process element abundances. The aforementioned chemical ratios provide a clear link between NGC 362 and GSE and Sausage stars, this is not the case for NGC 288. When fitting the two GCs with a GCE model designed to fit GSE stars, NGC 362 shows excellent agreement with a slightly altered model, while NGC 288 does not. We hypothesize that the two are either (i) not galactic siblings, and were therefore brought in via two separate, but perhaps similar events, or (ii) that chemical in $-$-homogenities across the GSE progenitor were large enough to create distinctions between GCs and galactic stars born at different spatial locations. This second point demands a larger degree of chemical inhomogeneity in the GSE progenitor than what is presently seen in the data. In the future, we would like to build a larger database of high precision comparisons between known GC siblings (found *in situ* around their birth galaxy) and/or comparisons between GCs and galactic member stars.

The two papers in this series represent the first high-precision differential chemical abundance analysis of multiple MW GCs. With errors as small as 0.01 dex we have delivered the most precise comparative/relative chemical abundance study ever undertaken of GCs. Coupled with high precision six-dimensional phase space measurements from *Gaia*, and thus orbits, this study is the most comprehensive relative chemo-dynamical GC study thus far. While it is not possible to unambiguously confirm or refute the conjecture that NGC 288 and NGC 362 are siblings, this pioneering study is a 'proof of concept' demonstration and builds the conceptual and analysis framework for future studies in this area.

In conclusion, NGC 362 and NGC 288 are remarkably similar chemically, but show distinct differences that dispute their joint association with GSE. We propose that either the two are not siblings or that GSE was chemically in-homogenous enough to explain the disagreements.

ACKNOWLEDGEMENTS

SM also wishes to acknowledge the traditional custodians of Mt. Stromlo, the Ngunawal and Ngambri people and pay her respect to elders past and present. SM acknowledges funding support from the Natural Sciences and Engineering Research Council of Canada (NSERC), [funding reference number PGSD3−545852–2020]. Cette recherche a été financée par le Conseil de recherches en sciences naturelles et en génie du Canada (CRSNG), [numéro de référence PGSD3−545852–2020]. This research was supported by the Australian Research Council Centre of Excellence for All Sky Astrophysics in 3 Dimensions (ASTRO 3D), through project number CE170100013.

This work relies heavily on the `Astropy` (Astropy Collaboration et al. 2013, 2018), `SciPy` (Virtanen et al. 2020), `NumPy` (Harris et al. 2020), and `Matplotlib` (Hunter 2007) libraries and `Jupyter` notebooks (Kluyver et al. 2016). Based on observations collected at the European Organisation for Astronomical Research in the Southern Hemisphere under ESO programme 075.D-0209(A).

DATA AVAILABILITY

The data underlying this article are available in Paper I in the supplementary material provided.

REFERENCES

Abadi M. G., Navarro J. F., Steinmetz M., 2006, MNRAS, 365, 747
Aguado D. S. et al., 2021, ApJ, 908, L8
Astropy Collaboration et al., 2013, A&A, 558, A33
Astropy Collaboration et al., 2018, AJ, 156, 123
Baumgardt H., Hilker M., 2018, MNRAS, 478, 1520
Baumgardt H., Vasiliev E., 2021a, MNRAS, 505, 5957
Baumgardt H., Vasiliev E., 2021b, MNRAS, 505, 5957
Baumgardt H., Hilker M., Sollima A., Bellini A., 2019a, MNRAS, 482, 5138
Baumgardt H., Hilker M., Sollima A., Bellini A., 2019b, MNRAS, 482, 5138
Belokurov V., Erkal D., Evans N. W., Koposov S. E., Deason A. J., 2018, MNRAS, 478, 611
Bennett M., Bovy J., 2019, MNRAS, 482, 1417
Binney J., Tremaine S., 2008, Galactic Dynamics: Second Edition. Princeton University Press, Princeton, New Jersey
Bisterzo S., Gallino R., Straniero O., Cristallo S., Käppeler F., 2011, MNRAS, 418, 284
Blanchard P. K. et al., 2017, ApJ, 848, L22
Bonaca A. et al., 2020, ApJ, 897, L18
Borre C. C. et al., 2022, MNRAS, 514, 2527
Bovy J., 2015, ApJS, 216, 29
Buder S. et al., 2021, MNRAS, 506, 150
Buder S. et al., 2022, MNRAS, 510, 2407
Buonanno R., Caloi V., Castellani V., Corsi C., Fusi Pecci F., Gratton R., 1986, A&AS, 66, 79
Burbidge E. M., Burbidge G. R., Fowler W. A., Hoyle F., 1957, Rev. Modern Phys., 29, 547
Busso M., Gallino R., Wasserburg G. J., 1999, ARA&A, 37, 239
Callingham T. M., Cautun M., Deason A. J., Frenk C. S., Grand R. J. J., Marinacci F., 2022, MNRAS, 513, 4107
Carretta E. et al., 2013, A&A, 557, A138
Chabrier G., 2003, PASP, 115, 763
Chilingarian I. V., Asa'd R., 2018, ApJ, 858, 63
Clarke J. P., Gerhard O., 2022, MNRAS, 512, 2171
Côté B., O'Shea B. W., Ritter C., Herwig F., Venn K. A., 2017, ApJ, 835, 128
Côté B. et al., 2018, ApJ, 855, 99
Côté B. et al., 2019, ApJ, 875, 106
Dalessandro E. et al., 2013, ApJ, 778, 135
Dehnen W., 2000, AJ, 119, 800
Dekker H., D'Odorico S., Kaufer A., Delabre B., Kotzlowski H., 2000, in Iye M., Moorwood A. F., eds, Soc. Photo-Optical Instrum. Eng. (SPIE) Conf. Ser., Vol. 4008, Optical and IR Telescope Instrumentation and Detectors. SPIE, Bellingham, Washington, p. 534
de los Reyes M. A. C., Kirby E. N., Ji A. P., Nuñez E. H., 2022, ApJ, 925, 66
Eilers A.-C., Hogg D. W., Rix H.-W., Ness M. K., 2019, ApJ, 871, 120
Fattahi A. et al., 2019, MNRAS, 484, 4471
Ferrers N., 1877, Quart. J. Pure Appl. Math, 14
Feuillet D. K., Feltzing S., Sahlholdt C. L., Casagrande L., 2020, MNRAS, 497, 109
Feuillet D. K., Sahlholdt C. L., Feltzing S., Casagrande L., 2021, MNRAS, 508, 1489
Forbes D. A., 2020, MNRAS, 493, 847
Forbes D. A., Bridges T., 2010, MNRAS, 404, 1203
GRAVITY Collaboration et al., 2019, A&A, 625, L10
Gaia Collaboration et al., 2018, A&A, 616, A1
Gaia Collaboration et al., 2021, A&A, 649, A1
Gaia Collaboration et al., 2022, preprint (arXiv:2208.00211)
Gallart C., Bernard E. J., Brook C. B., Ruiz-Lara T., Cassisi S., Hill V., Monelli M., 2019, Nat. Astron., 3, 932
Gnedin O. Y., Ostriker J. P., 1997, ApJ, 474, 223
Gustafsson B., Edvardsson B., Eriksson K., Jørgensen U. G., Nordlund Å., Plez B., 2008, A&A, 486, 951
Hammer F. et al., 2023, MNRAS, 519, 5059
Hansen C. J., Montes F., Arcones A., 2014, ApJ, 797, 123
Harris W. E., 1996, AJ, 112, 1487
Harris C. R. et al., 2020, Nature, 585, 357
Haywood M., Di Matteo P., Lehnert M. D., Snaith O., Khoperskov S., Gómez A., 2018, ApJ, 863, 113
Heggie D., Hut P., 2003, The Gravitational Million-Body Problem: A Multidisciplinary Approach to Star Cluster Dynamics. Cambridge University Press, Cambridge, UK
Helmi A., de Zeeuw P. T., 2000, MNRAS, 319, 657
Helmi A., Babusiaux C., Koppelman H. H., Massari D., Veljanoski J., Brown A. G. A., 2018, Nature, 563, 85
Hendricks B., Boeche C., Johnson C. I., Frank M. J., Koch A., Mateo M., Bailey J. I., 2016, A&A, 585, A86
Hill V. et al., 2019, A&A, 626, A15
Horta D. et al., 2020, MNRAS, 493, 3363
Horta D. et al., 2021, MNRAS, 500, 1385
Horta D. et al., 2022, MNRAS, 520, 5671
Hunter J. D., 2007, Comput. Sci.Eng., 9, 90
Ji A. P., Frebel A., Chiti A., Simon J. D., 2016, Nature, 531, 610
Karakas A. I., 2010, MNRAS, 403, 1413
Karakas A. I., Lattanzio J. C., 2014, PASA, 31, e030
Kluyver T. et al., 2016, in Loizides F., Schmidt B.eds, Positioning and Power in Academic Publishing: Players, Agents and Agendas. IOS Press, Amsterdam, Netherlands, p. 87
Kobayashi C., Karakas A. I., Lugaro M., 2020, ApJ, 900, 179
Koch-Hansen A. J., Hansen C. J., McWilliam A., 2021, A&A, 653, A2
Koppelman H. H., Helmi A., Massari D., Price-Whelan A. M., Starkenburg T. K., 2019, A&A, 631, L9
Kovalev M., Bergemann M., Ting Y.-S., Rix H.-W., 2019, A&A, 628, A54
Kruijssen J. M. D., Pfeffer J. L., Reina-Campos M., Crain R. A., Bastian N., 2019, MNRAS, 486, 3180
Law D. R., Majewski S. R., 2010, ApJ, 718, 1128
Leaman R., VandenBerg D. A., Mendel J. T., 2013, MNRAS, 436, 122
Lemasle B. et al., 2014, A&A, 572, A88
Letarte B. et al., 2010, A&A, 523, A17
Libralato M. et al., 2018, ApJ, 861, 99
Limberg G., Souza S. O., Pérez-Villegas A., Rossi S., Perottoni H. D., Santucci R. M., 2022, ApJ, 935, 109
Mackey A. D., Gilmore G. F., 2003, MNRAS, 338, 85
Mackey A. D., Gilmore G. F., 2004, MNRAS, 355, 504
Majewski S. R. et al., 2017, AJ, 154, 94
Malhan K., 2022, ApJ, 930, L9
Malhan K. et al., 2022, ApJ, 926, 107
Marín-Franch A. et al., 2009, ApJ, 694, 1498
Massari D., Koppelman H. H., Helmi A., 2019, A&A, 630, L4
Matsuno T., Aoki W., Suda T., 2019, ApJ, 874, L35
Matsuno T., Hirai Y., Tarumi Y., Hotokezaka K., Tanaka M., Helmi A., 2021, A&A, 650, A110
Matsuno T., Koppelman H. H., Helmi A., Aoki W., Ishigaki M. N., Suda T., Yuan Z., Hattori K., 2022a, A&A, 661, A103
Matsuno T. et al., 2022b, A&A, 665, A46
McKenzie M., Bekki K., 2021, MNRAS, 507, 834
McKenzie M. et al., 2022, MNRAS, 516, 3515
McMillan P. J., 2017, MNRAS, 465, 76
McWilliam A., Wallerstein G., Mottini M., 2013, ApJ, 778, 149
Meléndez J., Asplund M., Gustafsson B., Yong D., 2009, ApJ, 704, L66
Monari G., Famaey B., Siebert A., Grand R. J. J., Kawata D., Boily C., 2016, MNRAS, 461, 3835
Monty S., Venn K. A., Lane J. M. M., Lokhorst D., Yong D., 2020, MNRAS, 497, 1236
Monty S., Yong D., Marino A. F., Karakas A. I., McKenzie M., Grundahl F., Mura-Guzmán A., 2023, MNRAS, 518, 965
Mucciarelli A., Origlia L., Ferraro F. R., 2010, ApJ, 717, 277
Mucciarelli A., Origlia L., Ferraro F. R., Bellazzini M., Lanzoni B., 2012, ApJ, 746, L19
Mucciarelli A., Massari D., Minelli A., Romano D., Bellazzini M., Ferraro F. R., Matteucci F., Origlia L., 2021, Nat. Astron., 5, 1247
Myeong G. C., Evans N. W., Belokurov V., Sanders J. L., Koposov S. E., 2018, ApJ, 863, L28

Myeong G. C., Vasiliev E., Iorio G., Evans N. W., Belokurov V., 2019, MNRAS, 488, 1235
Myeong G. C., Belokurov V., Aguado D. S., Evans N. W., Caldwell N., Bradley J., 2022, ApJ, 938, 21
Naidu R. P., Conroy C., Bonaca A., Johnson B. D., Ting Y.-S., Caldwell N., Zaritsky D., Cargile P. A., 2020, ApJ, 901, 48
Naidu R. P. et al., 2022, ApJ, 926, L36
Nardiello D. et al., 2018, MNRAS, 481, 3382
Nissen P. E., Gustafsson B., 2018, A&A Rev., 26, 6
Nissen P. E., Schuster W. J., 2010, A&A, 511, L10
Ostriker J. P., Spitzer L., Jr., Chevalier R. A., 1972, ApJ, 176, L51
Pagnini G., Di Matteo P., Khoperskov S., Mastrobuono-Battisti A., Haywood M., Renaud F., Combes F., 2022, preprint (arXiv:2210.04245)
Paxton B., Bildsten L., Dotter A., Herwig F., Lesaffre P., Timmes F., 2011, ApJS, 192, 3
Piatti A. E., 2018, MNRAS, 473, 492
Pignatari M. et al., 2016, ApJS, 225, 24
Piotto G. et al., 2015, AJ, 149, 91
Ramírez I. et al., 2014, A&A, 572, A48
Recio-Blanco A., 2018, A&A, 620, A194
Ritter C., Côté B., Paul A., Herwig F., 2018a, Nugrid/Nupycee: Nupycee In Python 3, Zenodo
Ritter C., Côté B., Herwig F., Navarro J. F., Fryer C. L., 2018b, ApJS, 237, 42
Ritter C., Herwig F., Jones S., Pignatari M., Fryer C., Hirschi R., 2018c, MNRAS, 480, 538
Rosswog S., Korobkin O., Arcones A., Thielemann F. K., Piran T., 2014, MNRAS, 439, 744
Rostami Shirazi A., Haghi H., Khalaj P., Asl A. F., Hasani Zonoozi A., 2022, MNRAS, 513, 3526
Sakari C. M., McWilliam A., Wallerstein G., 2017, MNRAS, 467, 1112
Searle L., Zinn R., 1978, ApJ, 225, 357
Seitenzahl I. R. et al., 2013, MNRAS, 429, 1156
Shetrone M. D., Keane M. J., 2000, AJ, 119, 840
Shetrone M., Venn K. A., Tolstoy E., Primas F., Hill V., Kaufer A., 2003, AJ, 125, 684
Skúladóttir Á., Salvadori S., 2020, A&A, 634, L2
Skúladóttir Á., Hansen C. J., Salvadori S., Choplin A., 2019a, A&A, 631, A171
Skúladóttir Á., Hansen C. J., Salvadori S., Choplin A., 2019b, A&A, 631, A171
Sneden C., 1973, ApJ, 184, 839
Sollima A., 2020, MNRAS, 495, 2222
Spitzer L., Jr., 1969, ApJ, 158, L139
Sun G., Wang Y., Liu C., Long R. J., Chen X., Gao Q., 2023, Res. Astron. Astrophys., 23, 015013
Tolstoy E., Hill V., Tosi M., 2009, ARA&A, 47, 371
Trujillo-Gomez S., Kruijssen J. M. D., Reina-Campos M., Pfeffer J. L., Keller B. W., Crain R. A., Bastian N., Hughes M. E., 2021, MNRAS, 503, 31
VandenBerg D. A., Brogaard K., Leaman R., Casagrande L., 2013, ApJ, 775, 134
Vasiliev E., 2019, MNRAS, 482, 1525
Vasiliev E., Baumgardt H., 2021, MNRAS, 505, 5978
Virtanen P. et al., 2020, Nat. Methods, 17, 261
Webb J. J., Harris W. E., Sills A., Hurley J. R., 2013, ApJ, 764, 124
Wegg C., Gerhard O., Portail M., 2015, MNRAS, 450, 4050
Yong D. et al., 2013, MNRAS, 434, 3542
Young P. A. et al., 2006, ApJ, 640, 891
Yuan Z. et al., 2020, ApJ, 891, 39

APPENDIX A: ADDITIONAL CHEMICAL CORRELATIONS

Fig. A1 presents the differences between the two clusters in all possible element ratios, each coloured by significance. Interpretations for Fig. A1 are discussed in Section 3.2.2.

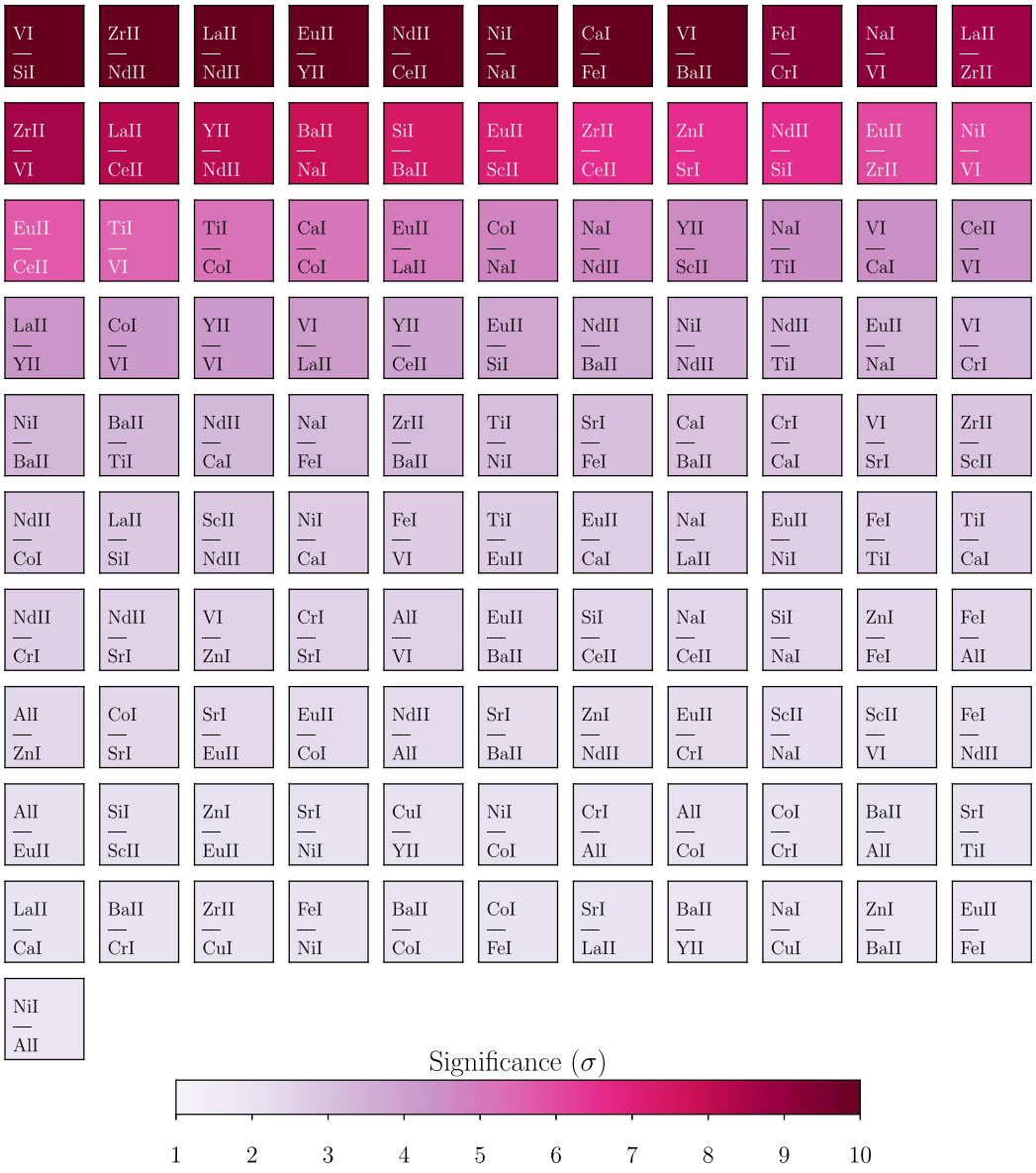

Figure A1. All possible element ratios coloured the statistical significance of the difference between the primordial *s*-weak group in NGC 362 and all stars in NGC 288. Note the differences in the ratio of the first peak *s*-process element Zr and the *r*-process element Nd between the clusters in addition to the differences in Y and Eu discussed in Section 3.2.2.

APPENDIX B: EXPLORING ORBITAL CHANGES TO NGC 362 UNDER THE ADDITION OF MW BAR

Fig. B1 shows the changes to the orbit of NGC 362 under three different MW potentials.

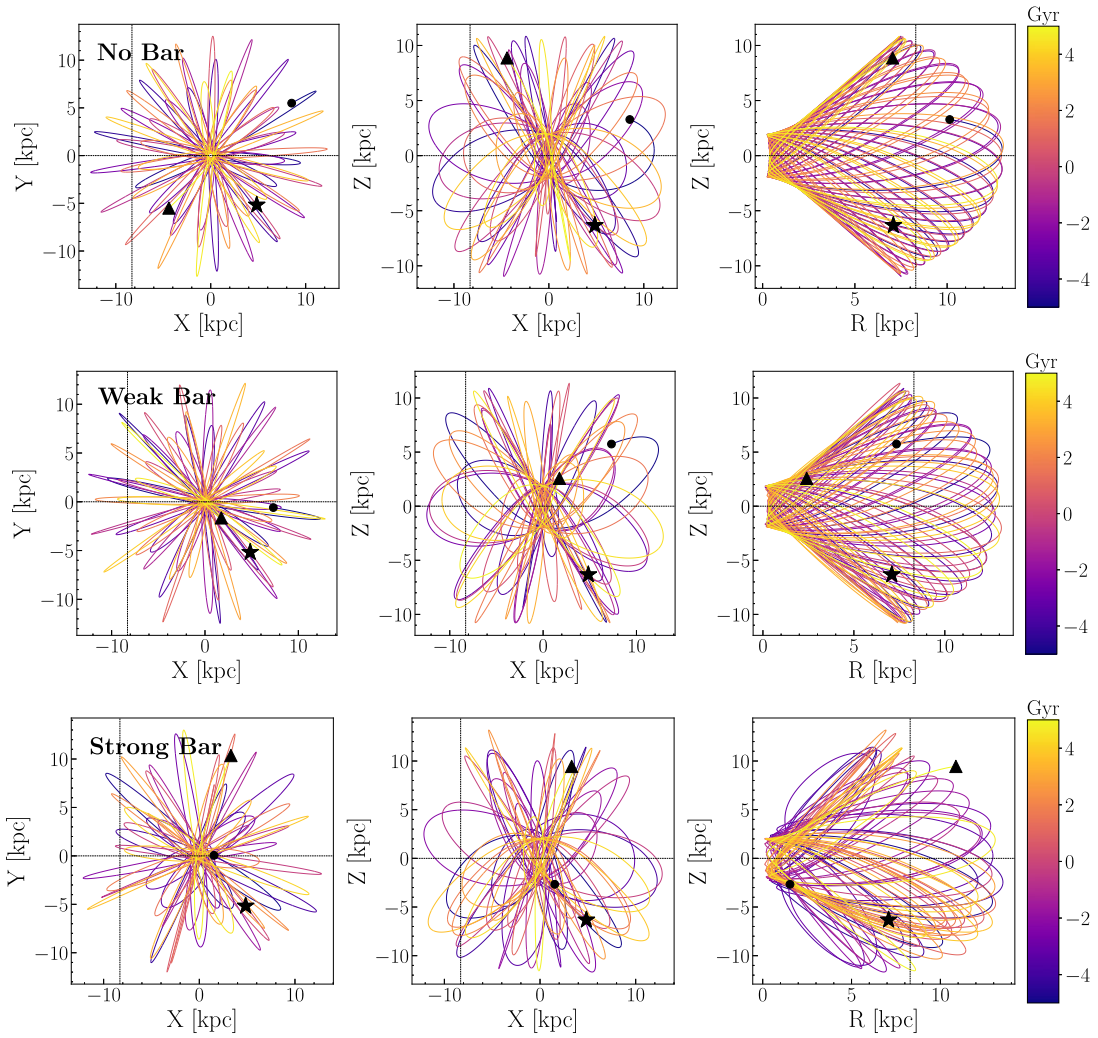

Figure B1. As in Fig. 2, for the GC NGC 362 integrated forwards and backwards for 5 Gyr in three different potentials. The position of the cluster 5 Gyr ago is marked with a circle, the present day position is marked with a star and the position 5 Gyr in the future is marked with a triangle. The trajectory is coloured by time and presented (from left to right) in the Y-X, Z-X and Z-R planes. *Top*, the orbit integrated in `MWPotential2014`, middle, integrated in `MWPotential2014 + DehnenBarPotential` with weak bar characteristics, bottom integrated in `MWPotential2014 + DehnenBarPotential` with strong bar characteristics. Details of the bar characteristics are given in Section 3.1.1. The position of the sun is marked with dashed lines.

This paper has been typeset from a TEX/LATEX file prepared by the author.